MATERIALS CHEMISTRY
FRONTIERS

REVIEW

View Article Online
View Journal | View Issue

Cite this: *Mater. Chem. Front.*, 2019, **3**, 2326

Ligand functionalized copper nanoclusters for versatile applications in catalysis, sensing, bioimaging, and optoelectronics

Shayan Shahsavari, †[ab] Samaneh Hadian-Ghazvini,†[c] Fahimeh Hooriabad Saboor,†[d] Iman Menbari Oskouie,[be] Masoud Hasany,[f] Abdolreza Simchi *[gh] and Andrey L. Rogach *[ij]

Received 30th July 2019,
Accepted 28th August 2019

DOI: 10.1039/c9qm00492k

rsc.li/frontiers-materials

Copper nanoclusters (Cu NCs) have emerged as a valuable member of the family of ligand-protected few-atomic metal nanoparticles and show fascinating properties of color-controlled light emission, combined with the advantages of versatile solution-based chemical synthesis at low cost. Synthetic methods of Cu NCs using various types of functional ligands and scaffolds allow tuning their emission wavelength and improving their environmental stability. Depending on the method of preparation and the ligands used, Cu NCs have already been applied for a wide variety of applications in catalysis, sensing, bioimaging, theranostics, and optoelectronics. This review highlights the potential of Cu NCs and links synthetic procedures and functionalization with different ligands with their properties and applications.

1. Introduction

Functional nanomaterials have undergone an impressive development and are now starting to impact diverse aspects of human life. An important class of nanomaterials is metal nanoparticles (NPs) with chemical, electrical, magnetic, and optical properties often different from their bulk phases,[1] which have made them applicable for a wide range of applications. A recent development in the synthesis of metal NPs is the fabrication of sub-nanometer structures which are composed of a few or few tens of atoms. These so-called metal nanoclusters (MNCs) provide a link between larger, plasmonic metal NPs and molecular-like compounds. Their sizes are close to the Fermi wavelength of electrons, so that they exhibit discrete electronic states and show fluorescence emission.[1–3] In recent years, many studies have been devoted to gold and silver NCs.[4] In spite of the lower cost and ready availability of copper, Cu NCs were more difficult to synthesize, while their photoluminescence quantum yields (PLQY) tended to be lower.[2] At the same time, the photostability of Cu NCs is better than that of organic dyes. In comparison with many II–VI and IV–VI semiconductor quantum dots with high PLQY, toxicity issues of Cu NCs are fewer,[4] while their cellular uptake could be easier, due to the smaller size.[5] Due to the useful chemical, optical and electrical properties of Cu NCs, efforts on broadening their applicability in various fields such as catalysts, chemical sensors, biological imaging agents, and electronic devices have increased in recent years.[2,3,6–8]

The aim of this article is to present a comprehensive review on the application-related aspects of Cu NCs (summarized in Table 1), which were not so much in the focus of other reviews. Recent advances in the synthetic protocols with an emphasis on their advantages and shortcomings are considered, and properties of Cu NCs related to several possible applications (Scheme 1) such as catalysis, detection and sensing, biological imaging, theranostics, and light emitting devices (LEDs) are discussed. The review concludes with the future trends and outlooks for the further development of the Cu NC field.

[a] *Department of Chemistry, Sharif University of Technology, Tehran, Iran*
[b] *Nanoclub Elites Association, Tehran, Iran*
[c] *Institute of Biochemistry and Biophysics, University of Tehran, Tehran, Iran*
[d] *Department of Chemical Engineering, University of Mohaghegh Ardabili, Ardabil, Iran*
[e] *School of Medicine, Tehran University of Medical Sciences, Tehran, Iran*
[f] *Department of Chemical and Petroleum Engineering, Sharif University of Technology, Tehran, Iran*
[g] *Department of Materials Science and Engineering, Sharif University of Technology, P.O. Box 11365-9466, 14588 Tehran, Iran. E-mail: simchi@sharif.edu; Fax: +98 (21) 6600 5717; Tel: +98 (21) 6616 5226*
[h] *Institute for Nanoscience and Nanotechnology, Sharif University of Technology, P.O. Box 11365-9466, 14588 Tehran, Iran*
[i] *Department of Materials Science and Engineering, and Centre for Functional Photonics, City University of Hong Kong, 83 Tat Chee Avenue, Kowloon, Hong Kong S.A.R. E-mail: andrey.rogach@cityu.edu.hk*
[j] *Shenzhen Research Institute, City University of Hong Kong, Shenzhen, 518057, China*
† These authors contributed equally to this work.

Table 1 A summary of versatile applications of Cu NCs produced by different synthetic methods

Application	Synthesis method	Cu NCs	Cluster formula	Type of reaction	Reactant	Product	Year	Ref.
Catalysis	Ligand assisted	D-Penicillamine capped Cu NCs	Cu_6L_4(L = D-penicillamine)	Reduction	Methylene blue	Lucomethylene blue	2014	9
		1-Dodecanethiol capped Cu NCs	Cu_8DT_8	Reduction	O_2	OH*	2014	10
		Tetraoctylammonium formate capped Cu NCs	—	1,3-Dipolar cycloaddition	Azides and terminal alkynes	1,2,3-Triazoles	2005	11
		Double ligand capped Cu NCs	$[(Cu_{20}(CCPh)_{12}(OAc)_6)]$ supported on silica	1,3-Dipolar cyclo addition	Azides and terminal alkynes	1,2,3-Triazoles	2018	12
	Protein templated	BSA–Cu NCs	—	Oxidation	Styrene	Benzaldehyde	2014	13
	Photo-reduction	Cu/CuO NCs on TiO_2 nanotube arrays	—	Reduction	Methylene blue 4-Nitrophenol	Lucomethylene blue 4-Aminophenol	2017	14
	Physical	Cu NCs deposited on MgO	—	Reduction	4-Nitrophenol	4-Aminophenol	2018	15
		Cu NCs based on the decomposition of surface	—	HER	CO and H_2O	H_2 and CO_2	2016	16
	Hydro-thermal	Cu NCs loaded on nanocrystalline Cr_2O_3	—	Oxidation	Cyclohexane	Cyclohexanone	2012	17

Application	Synthesis method	Cu NCs	Cluster formula	Target	Limit of detection (LOD)	Linear range	Year	Ref.
Sensors	Organic polymer-templated	PEI–Cu NCs	—	TNT	14 pM, 0.05 nM	0–8 nM	2018	18
		PVP–Cu NCS	$Cu_{11}L_{10}$ $[Cu_{12}L_{10} + 3H] + [Cu_{13}L_{11} + H]$ + L = *N*-vinyl-pyrrolidone	Trinitrophenol	0.391 μM	0–27 μM	2019	19
		PVP-protected Cu NCs	—	Temperature	—	20–75 °C	2017	20
		PVP-protected Cu NCs	—	Glutathione (GSH)	17 μM	0–0.14 mM	2019	21
		PEI–Cu NCs	—	pH	—	2.0–13.2	2016	22
		PEI–Cu NCs	—	Cysteine	0.34 μM	1–25 μM	2018	23
		PEI–Cu NCs	—	Protein kinase	0.038 U mL^{-1}	0.1–6.0 U mL^{-1}	2017	24
	Protein/ peptide-templated	Ovalbumin-directed Cu NCs	—	Doxycycline	270 pM	1–1000 μM	2018	25
		BSA–Cu NCs/MOF	—	Tramadol	0.8 nM	0.003–2.5 μM	2019	26
		BSA–Cu NCs	—	RDX	1.62 nM	0–0.238 μM	2019	27
		Silk fibroin–Cu NCs	—	S^{2-}	0.3 μM	5–110 μM	2019	28
		BSA–Cu NCs	—	Gossypol	25 nM	0.1–100 μM	2019	29
		Metallothionein–Cu NCs	—	Hg^{2+} Pb^{2+}	43.8 nM 142.0 nM	97 nM–2.3 μM 0.7–96 μM	2019	30
		Natural silk fibroin-stabilized Cu NCs (SF@Cu NCs)	—	pH	—	6.08–10.05	2016	31
		Human serum albumin (HSA) templated Cu NCs	—	Bilirubin	3.5×10^{-8} M 1.45×10^{-7} M	1.25×10^{-6} to 7.50×10^{-6} M 5.00×10^{-6} to 2.875×10^{-5} M	2019	32
		Carbon dots/BSA–Cu NCs	—	Dopamine	32 nM	0.1 to 100 μM	2018	33
		BSA–Cu NCs	—	Rutin	0.02 μM	0.1–100 μM	2018	34
		BSA–Cu NCs	—	Protamine Heparine	0.12 ng mL^{-1} 0.0406 ng mL^{-1}	3–12 ng mL^{-1} 6–9 ng mL^{-1}	2019	35
		Ovalbumin stabilized Cu NCs	—	Folic acid	0.18 μM	0.5–200 μM	2019	36
		Cu NC-encapsulated liposomes	—	Cardiac Troponin T (cTnT) antigen	0.03 pg mL^{-1}	0.1 to 2 pg mL^{-1}	2018	37
	DNA-templated	Reticular DNA template Cu NCs	—	Hg^{2+}	16 pM	50 pM–500 μM	2018	38
		TCSDA and dsDNA-templated Cu NCs	—	ATP	5 pM	0.01–100 nM	2017	39
		dsDNA–Cu NCs/GO	—	Protein kinase	0.039 U L^{-1}	0.1–5 U L^{-1}	2018	40
		poly-(T) ssDNA templated Cu NCs	—	Uracil-DNA glycosylase (UDG)	5.0×10^{-5} U mL^{-1}	$1.0 \times 10^{-4} \times 0.01$ U mL^{-1}	2019	41
		dsDNA templated Cu NCs	—	Human immunoglobulin G (IgG)	7 pg mL^{-1}	0.05–12 ng mL^{-1}	2019	42
		dsDNA templated Cu NCs	—	T4 polynucleotide kinase phosphatase	0.06 U mL^{-1}	0.07 U mL^{-1} to 15 U mL^{-1}	2019	43

Table 1 (*continued*)

Application	Synthesis method	Cu NCs	Cluster formula	Target	Limit of detection (LOD)	Linear range	Year	Ref.
		ssDNA bivalent aptamer–Cu NCs	—	Vascular endothelial growth factor (VEGF)	12 pM	10–800 pM	2019	44
		ssDNA (elongated poly(T))-templated Cu NCs	—	Biotin	3.1 nM	10–1000 nM	2017	45
		ssDNA (elongated poly(T))-templated Cu NCs	—	Streptavidin	0.47 nM	1–200 nM	2017	45
		ssDNA (elongated poly(T))-templated Cu NCs	—	Uracil-DNA Glycosylase (UDG) Activity	0.00005 U mL^{-1} 0.000002 U mL^{-1} (hyperbranched DNA templates)	0.00005–0.002 U mL^{-1}	2019	46
		DNA-templated Cu NCs	—	MicroRNA-155	1.1 × 10^{-11} M	5.0 × 10^{-11} M to 1.0 × 10^{-8} M	2017	47
		Hairpin DNA-templated Cu NCs	—	MicroRNA-155	2.2 × 10^{-12} M	5.0 × 10^{-12} to 1.0 × 10^{-8} M	2017	48
		DNA-templated Cu NCs	—	Abasic sites in dsDNA	1 lesion in 74 nucleotides	—	2018	49
		AT-rich dsDNA-template Cu NCs	—	microRNA	36 aM	—	2018	50
	Ligand-assisted	Cysteine–Cu/Mo NCs	—	Methotrexate	13.7 nM	50 nM–100 μM	2019	51
		CTAB–Cu NCs	—	Carbamazepine	0.08 μg mL^{-1}	0.2–20 μg mL^{-1}	2019	52
		Dithiothreito–Cu NCs/carbon nitride nanosheets	—	Hg^{2+}	0.01 nM	0.5–10 nM	2019	53
		GSH–Cu NCs	—	*o*-Phenylenediamine (OPD)	93 ng L^{-1}	0.15–110 μg L^{-1}	2019	54
		L-Cys–Cu NCs	$Cu_4(Cys)_{3-5}$	*m*-Dinitrobenzene	0.13 μM	99 nM–1.3 μM	2019	55
		Cys–Cu NCs–DPA	—	Folic acid	68.9 nM	0.1–10 μM	2019	56
				Nitrite	95.4 nM	0.1–80 μM		
		GSH–Cu NCs	—	Cu^{2+}	0.17 μM	—	2019	57
		Bi-ligand (thiosalicylic/cyste-amine)–Cu NCs	—	Cr^{6+}	0.03 μM	0.1–1000 μM	2019	58
		GSH–Cu NCs/carbon dots	—	Humidity	—	40–80%	2019	59
		AMTD–Ac–Cu NCs	Cu_3L, Cu_3LX, Cu_3LX_2	H_2O	0–25.92 v/v%	0.036% (EtOH) 0.018% (THF) 0.024% (ACT) 0.026% (MeCN)	2018	60
		AMTD: (2-amino-5-mercapto-1,3,4-thiadiazole)	L = AMTD X = Ac					
		Adenosine-stabilized Cu NCs	—	Nitrofurantoin	30 nM	0.05–4 μM	2018	34
		Cysteamine-capped Cu NCs	—	Al^{3+}	26.7 nM	1–7 μM	2018	61
		Curcuma root extract (CRE)–Cu NCs	—	Hg^{2+}	0.12 nM	0.0005–25 μM	2018	62
		D-Penicillamine-coated Cu/Ag alloy NCs	$[Cu_3Ag_2L_4 + H]^+$ $[Cu_2Ag_2L_3 + H]^+$ $[Cu_3AgL_3 + H]^+$ $[Cu_2Ag_2L_2 + Na]^+$ L = D-penicillamine	Ag^+	5.9 μmol L^{-1}	0–0.79 mmol L^{-1}	2018	63
				Halides	—	095–1.72 mM		
		Cytidine-protected Cu NCs	—	$Cr_2O_7^{2-}$	24 nM	0.05–7.0 μM L^{-1}	2017	64
		Thiosalicylic acid (TA) capped Cu NCs	—	CN^-	5 nM	0.01–1 μM	2017	65
				NO_2^-	5 μM	15–50 μM		
		Bimetallic Cu/Ag NCs	—	Temperature	—	4–55 °C	2017	66
		D-Penicillamine–Cu NCs	—	Acid phosphatase	0.8 U L^{-1}	2.2–45.5 (100) U L^{-1}	2017	67
		4-Methylthiophenol-capped Cu NCs	—	β-Galactosidase	0.9 U L^{-1}	2.5–212.0 U L^{-1}	2017	68
		L-Histidine protected Cu NCs	—	Alkaline phosphatase	45 μU mL^{-1}	0.5 mU mL^{-1} to 40 mU mL^{-1}	2019	69

Table 1 (*continued*)

Application	Synthesis method	Cu NCs	Cluster formula	Target	Limit of detection (LOD)	Linear range	Year	Ref.
		GSH–Cu NC	Cu_2L_4 Cu_4L_3,(L = $C_{10}H_{16}O_6N_3S$)	Glucose	3.2×10^{-5} M	0.1–2.0 mM	2019	70
	Etching	L-Cysteine Cu NCs	—	TNT	9.1 nM	0–4.8 μM	2017	71

Application	Synthesis method	Cu NCs	Cluster formula	Target	$\lambda_{ex}/\lambda_{em}$	PL QY	Year	Ref.
Imaging and theranostics	Organic polymer-templated	α-Methoxy-ω-thioacetate poly(ethylene glycol) capped Cu NCs	—	Nuclear staining of DNA in HeLa cell line	390 nm, 500 nm, and530 nm/583 nm	30% in water 67% in THF	2015	5
	Protein/peptide-templated	Egg white capped Cu NCs	—	*Bacillus subtilis* cells	344 nm/600 nm	6.7%	2016	72
	Ligand-assisted	GSH capped Cu NCs	—	Thermometry inside MDA-MB-231 cell line	400 nm/610 nm	4.5%	2017	73
	Ligand-assisted	Folic acid modified Cu NCs	—	HeLa cell line	350 nm/440 nm	11.6%	2018	74
	Ligand-assisted/organic polymer-templated	Cysteine-stabilized Cu NCs in chitosan matrix	C_5L C_6L L = L-cysteine	MCF-7 and HEK 293 cell line	405 nm/488 nm	—	2018	75
	Protein/peptide-templated	^{64}Cu NC@BSA-LHRH.	—	Orthotopic lung tumors	680 nm/740 nm	—	2015	76
	Protein/peptide-templated	Tf-Stabilized Cu NCs	—	Tf receptor positive Daltons lymphoma ascites bearing mice	375 nm/460 nm	—	2018	77
	Ligand-assisted	^{64}Cu NCs functionalized with temozolomide	—	Glioblastoma	—	—	2018	78
	Organic polymer-templated	PVP-templated Cu NCs	$Cu_{11}L_{10}$ $Cu_{12}L_{11}$ $Cu_{13}L_{11}$ L = PVP	THP-1 macrophages	392 nm/618 nm	44.67%	2019	19

Application	Synthesis method	Cu NCs	Cluster formulation	Morphology	$\lambda_{ex}/\lambda_{em}$	PL QY	Year	Ref.
Light harvesting	Ligand-assisted	Cysteine capped Cu NCs	Cu_7L_3 L = L-cysteine	Spherical	365 nm/489 nm	6.2%	2018	79
Solar cells		Double ligand capped Cu NCs	$[Cu_{53}(RCOO)_{10}(CCtBu)_{20}Cl_2H_{18}]^+$	Spherical	—	—	2019	80
LEDs		1-Dodecanethiol capped Cu NCs	$Cu_{14}DT_{10}$	Nano sheets	365 nm/400–700 nm	6.5%	2015	81
		Thiophenol based compounds stabilized Cu NCs	Cu_9L_7 Cu_8L_8 Cu_9L_6 Cu_8L_6 $Cu_{10}L_{10}$ L = 4-X thiophenol	Nano ribbons	365 nm/400–700 nm	15.6%	2017	82
		GSH capped Cu NCs in a biopolymeric matrix	—	Nano aggregates	365 nm/600 nm	42%	2018	83
		Ce^{3+} crosslinked L-cysteine capped Cu NCs	—	Mesoporous Spheres	395 nm/617 nm	8.3%	2018	84
	Organic polymer-templated	PVP–Green Cu NCs with DHLA	—	Spherical	398 nm/491 nm	2.46%	2019	85
		PVP–Green Cu NCs with DHLA Red Cu NCs	—	Nano aggregates	424 nm/610 nm	4.83%		

Scheme 1 Schematic depiction of different possible applications of copper nanoclusters.

2. Optical properties of metal NCs and their aggregation/assembly induced emission

The ultrafine size (usually less than 2 nm) of metal NCs induce electronic transitions between separated energy levels giving rise to light absorption at a given wavelength and emission with a longer wavelength.[2,86,87] Bornacelli and coworkers[88] synthesized bare Pt, Ag and Au NCs by ion-implantation in sapphire plates, and employed the Jellium model, $E_{Fermi}/N^{1/3}$, to simulate their emission spectra. They concluded that the optical emission of these clusters can be explained based on the quantum confinement effects. Hovewer, the Jellium model would not work for ligand-functionalized NCs such as the thiolate-protected ones, because it does not take into account the contribution of ligands towards the electronic structure and the optical transitions of such structures. The PL origin of ligand-protected metal NCs and relevant parameters that contribute to their emission have been summarized by Xie and co-workers in a recent book,[89] pointing out the effect of varying core sizes and the type of ligands.[90] Ligand exchange further confirmed their effects on the PL of metal NCs.[91] Besides the effects of the ligands and the metal core, there are some other variables such as the thiol-to-metal ratio and the oxidation state of the metal core that affect the PL response of metal NCs.[89]

It has been demonstrated in a plenty of studies that the emission of the metal NCs can be significantly improved as a result of their aggregation. The aggregation-induced emission (AIE) phenomenon which was discovered for molecular dyes in 2001 by Tang and coauthors is also valid for the metal NCs, so far.[89,92] AIE characteristics of the metal NCs include sufficiently high PL QYs (typically in the range of 10–50%), large Stokes shift, and long excited state lifetimes.[89,93] Among the different ligand stabilized metal NCs, those capped with glutathione, 1-dodecanethiol, penicillamine, and cysteine are the most often reported ones with AIE. The AIE effect in metal NCs can be conveniently triggered by post-synthetic treatment, when changes of the solvent polarity, pH, and/or addition of some ions induce their self-assembly and aggregation.[89,92] Although the exact mechanism of AIE in metal NCs still requires further studies, it has been generally stated that

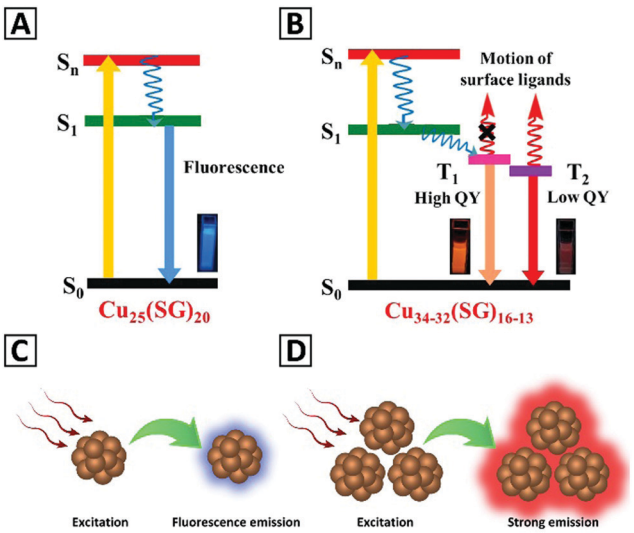

Fig. 1 Schematics of the energy levels and excitation/emission processes in (A) isolated $Cu_{25}(SG)_{20}$ NCs and (B) aggregated $Cu_{34-32}(SG)_{16-13}$ NCs. Adapted with permission from ref. 92, Copyright 2019, ACS. (C and D) Give a schematic representation of the emission from the isolated metal NCs and the aggregated clusters, respectively.

restriction in molecular rotational and vibrational motions of the capping ligands after aggregation blocks non-radiative pathways and opens radiative ones, and thus subsequently leads to PL enhancement. As illustrated in Fig. 1, the emission of isolated metal NCs relies on the S_1 to S_0 transition (fluorescence), while aggregated ones emit based on the T_1 to S_0 transition (phosphorescence).[89,92,94] An additional advantage of the AIE of aggregated metal NCs is that their emission color often appears in the red and near-infrared spectral regions, which means they can be employed for biosensing, with little interference with the autofluorescence of biological materials.[94]

3. Synthesis of copper NCs

Fig. 2A and Table 1 summarize the main chemical and physical preparation methods that have been utilized for the synthesis

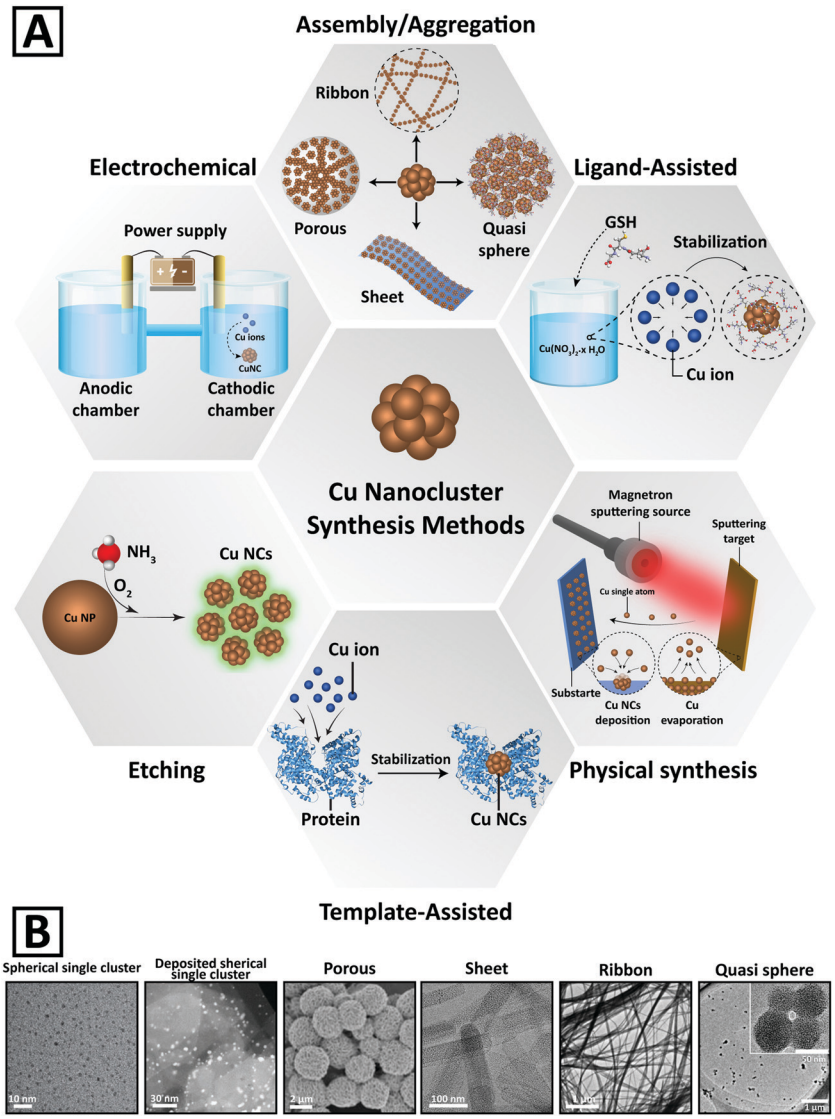

Fig. 2 (A) Schematic representation of different chemical and physical methods developed for the synthesis of Cu NCs. (B) Representative electron microscopy images of Cu NCs with different morphologies. Adapted with permission from ref. 15, 82, 84 and 100–102, Copyrights 2016–2018, Wiley-VCH, RSC, and ACS.

of Cu NCs so far. The synthetic procedures can be categorized into 6 groups, including ligand assisted, template-assisted, electrochemical, etching, and physical methods, and assembly and aggregation.[64] Chemical methods rely on the reduction of Cu^{2+} ions into Cu atoms in a solution phase.[95,96] Ligands and templates are often employed to stabilize the clusters and to protect them from aggregation and oxidation;[2,5,97,98] therefore, assembly and aggregation are considered as a subset of the ligand assisted method, which results in two- and three-dimensional cluster morphologies. Representative electron microscopy images of Cu NCs with different morphologies are presented in Fig. 2B.

Several characterization protocols of Cu NCs are in place to confirm different aspects of their structure. NMR spectroscopy and X-ray absorption spectroscopy are often used, as are chromatographic methods to assess their purity.[99] X-ray photoelectron spectroscopy (XPS) is applied to study the oxidation states of the metallic core of Cu NCs, while it has to be noted that the unambiguous recognition between Cu(0) and Cu(I) states is challenging.[79] Absorption and steady-state/time-resolved PL spectroscopy are routine while essential measurements to provide basic optical characterization of NCs, and for the determination of their PLQY.[92]

3.1. Ligand assisted synthesis of Cu NCs

During the synthesis and formation of Cu NCs, there is a high tendency of aggregation in order to decrease the surface energy, and ligands can prevent this by steric effects which rely on non-bonding interactions. Ligands can also influence the reactivity of precursor ions and molecules, which determines the final size and shape of NCs.[103] Controlling the kinetics of Cu^{2+} reduction in the presence of ligands is crucial to attain monodisperse Cu NCs. Different parameters such as ligand concentration, reducing agent

concentration, the pH of solution, the temperature, and the reaction time can affect the formation of desirable products. Choosing different ligands not only affects the PL intensity and the catalytic activity of ligand functionalized Cu NCs, but also plays a role in sensitivity to various environments.[104] Ligands with thiol and carboxyl groups are the two most important organic molecules which have widely been utilized for the synthesis of Cu NCs,[64] as will be presented below.

3.1.1. Thiolate ligands. Many research groups have employed glutathione (GSH) as a ligand for the synthesis of Cu NCs. Huang *et al.*[105] synthesized GSH-capped Cu NCs which had a red luminescence under UV irradiation at 365 nm. Wang *et al.*[98,106] used GSH as both protecting and reducing agents, mixing GSH and Cu^{2+} with a molar ratio of 4 : 1 which resulted in Cu NCs with a red emission at 600 nm. Mukherjee and co-workers[107] mixed Cu^{2+} and GSH with a molar ratio of 1 : 1 and prepared Cu NCs ($Cu_{15}(GSH)_4$) having a blue emission under UV irradiation. Through a similar approach, Huang *et al.*[108] synthesized Cu NCs with an intense blue fluorescence under 365 nm UV irradiation. They added ascorbic acid (AA) to a solution of Cu^{2+} and GSH and stirred the mixture for 4 h at 65 °C/pH = 6. Cu NCs with a red emission at 620 nm under UV excitation (365 nm) were also prepared by mixing GSH and Cu^{2+} at a molar ratio of 5 : 1. The maximum PLQY (24%) was attained at pH = 5.[101,109]

More recent advances are the synthesis of GSH-capped Cu NCs with different sizes by heating the solution (up to 80 °C) under N_2 flow, followed by separation of clusters through gel electrophoresis, capillary electrophoresis, and liquid chromatography. The resulting Cu NCs had a composition of Cu_5 $(GSH)_6$, $Cu_6(GSH)_6$, $Cu_7(GSH)_6$, $Cu_8(GSH)_6$, and $Cu_9(GSH)_6$. We note that some of these Cu NCs have larger sizes than Au_{25} $(GSH)_{18}$ prepared by gel electrophoresis.[110] Han *et al.*[111] developed a one-pot synthesis protocol to prepare GSH-protected Cu NCs encapsulated in metal–organic frameworks (MOFs). To obtain Cu NCs@GSH/MOF-5, 1,4-benzene dicarboxylic acid and Zn $(NO_3)_2.6H_2O$ were dissolved in DMF, and under stirring Cu^{2+} salt and GSH solutions were introduced. Through adjusting pH to 5, a white turbid solution was attained after 24 h at room temperature (RT). The fluorescence intensity of Cu NCs in the composite nanostructure was enhanced 35-fold, while the stability improved from 3 days to 3 months.

Another approach utilizes thiolates as ligands for an organic-phase synthesis of GSH stabilized Cu NCs with a red PL emission under UV irradiation. Huang *et al.*[112] prepared Cu NCs in DMF by a simple mixing method and used them for sensitive detection of water in organic solvents. GSH capped Cu NCs were synthesized by injection of a saturated GSH aqueous solution into a solution of Cu^{2+} in EtOH, and the aggregation was triggered by supersaturation of GSH in EtOH as a poor solvent. The PL QY was 48% in the solid state, which exceeded the value reported for Zn-coordinated GSH-capped Au NCs.[93,113]

Zhao and co-workers[67] used D-penicillamine as a suitable ligand for the synthesis of Cu NCs. They obtained Cu NCs with a bright red luminescence at 37 °C and at an incubation time of 4 min. Other groups also used penicillamine as a protecting ligand for the synthesis of Cu NCs.[9,114–116] Chen and co-workers[96] used 2-mercapto-5-*n*-polypyrimidine as a ligand and $NaBH_4$ as a reducing agent. They obtained clusters with the composition of $[Cu_8(C_7H_9N_2S)_4]$ which had PL with dual emissions at 423 nm and 593 nm and PLQY of 3.5% and 0.9%, respectively. Chang's group[65] has shown that thiosalicylic acid can also be used as a ligand; by mixing it with THF in DMF and then adding Cu^{2+}, Cu NCs were obtained. Mercaptosuccinic acid (MSA) was also utilized as a ligand in the presence of $NaBH_4$ as a reducing agent.[117] Another molecule that has often been used as a ligand is L-cysteine. Borghei *et al.*[118–120] have shown that Cu NCs can rapidly be prepared in the presence of cysteine at pH = 12 at RT, which exhibited a PL emission in the range of 410 to 580 nm depending on the cysteine concentration. Su and Liu[121] employed L-cysteine with an equal molar ratio with Cu^{2+} to prepare Cu NCs with a pale red emission color under UV irradiation (365 nm). Blue emitting Cu NCs (at 428 nm) were prepared with 4,6-diamino-2-mercaptopyrimidine (DAMP) as a ligand by Khonkayan *et al.*[122] Stable red emissive Cu NCs were fabricated from $CuCl_2$ using L-cysteine as a capping ligand and a mild reducing agent at RT.[121] These pH responsive Cu NCs were used for producing hybrid nanostructures with bovine serum albumin (BSA), which were soluble in water at pH = 3.0 and had PLQY of 6.3% and 2.1% in the solid state and aqueous solution, respectively.[121]

The cation cross-linking procedure has been used to fabricate aggregated L-cysteine capped Cu NCs with a mesoporous morphology and improved PLQY.[84] For this purpose, 100 μL of 0.1 M $CuSO_4{\cdot}5H_2O$ was added to 2 mL of 0.1 M L-cysteine in water; the mixture was subjected to vortexing for 10 min, and a suitable amount of 0.1 M Na_2CO_3 was added to induce aggregation. Thereafter, different amounts of Ce^{3+} were titrated to produce cross-linked aggregates; PLQY before and after Ce^{3+} addition was 3.4% and 8.3%, respectively.[84] Yet another strategy for improving the PLQY of Cu NCs is direct metal doping. For example, central doping of Au as a single atom into dichalcogenolate-protected Cu NCs led to strong enhancement of their PLQY, which reached 59% when measured at 77 K in 2-MeTHF for $[Au@Cu_{12}(S_2CN^nBu_2)_6(CCPh)_4]^+$ clusters.[123]

Self-assembly of Cu NCs into wires, ribbons, and sheets has been realized by employing 1-dodecanethiol (DT) as a ligand. For the synthesis of ribbons, for example, 30 mg of copper(II) acetylacetonate was dissolved in a mixture of dibenzyl ether (2 mL) and liquid paraffin (5 mL). Then, 1 mL DT was introduced, and the mixture was stirred at 120 °C for 30 min.[10]

Several other thiolate ligands were also employed for the synthesis of Cu NCs, namely, cysteamine,[124,125] phenylethanethiol,[114] dihydrolipoic acid,[126] mercaptobenzoic acid,[127] 3-mercapto-trimethoxy silane,[128] and 2-mercapto-1-methylimidazole.[129]

3.1.2. Ligands with carboxyl groups. Ligands with carboxyl groups are less frequently used for the synthesis of Cu NCs. As an example, Cu NCs were prepared by mixing Cu^{2+} and sodium cholate at controlled concentrations to form blue hydrogels. The PL spectra displayed the maximum excitation wavelength at 375 nm and an emission peak at 615 nm.[130] Tannic acid as a ligand and AA as a reducing agent have been used to make Cu NCs exhibiting a blue PL emission at 430 nm under excitation at 360 nm.[4] Zheng *et al.*[131] showed that AA itself can serve as a

protecting ligand upon the synthesis of Cu NCs when the reaction mixture was kept for 3 h at 25 °C.

3.2. Template-assisted synthesis of Cu NCs

To prepare Cu NCs and at the same time avoid their aggregation, templates such as DNA, protein, peptides, and polymers have been widely utilized. Cu^{2+} ions are able to bind to those templates and are then reduced to form clusters, whose aggregation is prevented by steric hindrance. Different templates can be chosen based on the types of potential application. Parameters such as pH, temperature, ratio of Cu^{2+} and templates can control the ratio of functional ligand groups and the metal core. For example, in Cu NC synthesis utilizing the protein template, the increase of pH facilitates breaking of disulfide bonds and stabilizes Cu NCs within the protein scaffold by thiol groups. A recent study has shown that by modifying the synthetic conditions in the template-assisted method, high PLQY exceeding 44% in water can be achieved.[19] A brief overview of the resulting Cu NCs is given below.

3.2.1. DNA templating. DNA templates have widely been employed for the synthesis of Cu NCs. Borghei *et al.*[48] synthesized orange- and green-emitting DNA–Cu NCs using ascorbate as the reducing agent for Cu^{2+} ions in phosphate buffer saline (PBS) at pH ~ 7. Mokhir's group[132] utilized AA as the reducing agent and double-stranded DNA (dsDNA) as the template to obtain Cu NCs with a strong PL emission in the range of 580–600 nm. Similarly, Singh *et al.*[49] used two single-stranded DNA (ssDNA) to prepare dsDNA in the presence of AA and employed them to grow Cu NCs. Han *et al.*[133] prepared thymine(T)-template fluorescent Cu NCs through the reduction by $NH_2OH{\cdot}HCl$ at pH 11.5, which exhibited a strong PL peak at 561 nm when excited at 354 nm. In a similar study, Cu NCs with a PL emission of 617 nm (for excitation at 349 nm) were prepared using elongated poly T as a template.[45] The template was prepared *via* polymerization of T with biotin-DNA/folate-DNA as the primer, and terminal deoxynucleotidyl transferase (TdT) as the catalyzing enzyme. The mixture was allowed to react in the PCR tube for 4 h at 37 °C. In another study,[134,135] Zhou's group showed that DNA with long chains can stabilize Cu NCs at RT within 2.5 h. Herein, TdT was used to polymerize DNA in the presence of adenine and thymine at a molar ratio of 1 : 1. Examination of different ssDNA templates like random ssDNA, poly A, poly T, poly C and poly G at pH 7.6 by 3-morpholinopropane-1-sulfonic acid has indicated that only poly T template yielded luminescent Cu NCs with a PL peak at ~600 nm when excited at 340 nm.[97,136] The reason for this is that Cu^{+} is an intermediate product of Cu^{2+} reduction to Cu, and T has the lowest affinity for binding to Cu^{+} (while G has the highest affinity for binding to Cu^{+}).

3.2.2. Polymer templating. Polyethyleneimine (PEI) has widely been utilized as a template for the synthesis of Cu NCs, while hydrazine hydrate[137] and AA[138] were the most popular reducing agents for reduction of Cu^{2+} to Cu atoms in combination with PEI. For instance, Cu NCs@PEI with an intense blue emission under excitation at 365 nm have been prepared by mixing a Cu^{2+} solution, AA and PEI, followed by microwave irradiation for 20 s and incubation at 25 °C for 3 h.[18,137] Poly(amidoamine) (PAMAM) dendrimers as a template and $NaBH_4$ as the reducing agent have also been utilized to prepare Cu NCs with different number of Cu atoms in the core, ranging from 4 to 64.[139–141] Bologh *et al.*[142] employed a polypropylene imine dendrimer modified with diaminobutane, and $NaBH_4$ in methanol as a reducing agent to produce Cu NCs. Polyvinylpyrrolidone (PVP) was used as the template in the presence of AA and formaldehyde (as the reducing agent) to prepare Cu NCs with 398–457 nm PL emission under UV irradiation (310 nm to 390 nm).[143,144] Some reducing agent free methods have also been examined. For instance, poly(methacrylic acid) modified with pentaerythritol tetrakis 3-mercaptopropionate has been used as a template for the synthesis of Cu NCs *via* photo-reduction of Cu^{2+}, yielding clusters with a PL emission peak of 630 nm under excitation at 360 nm.[145] Polyethylene glycol (PEG) modified with lipoic acid has been used to prepare blue emitting Cu NCs.[5] Green emitting water-soluble Cu NCs with a high PLQY of ~44% were synthesized through introducing an aqueous solution (10 mL) of 100 μL $CuCl_2$, 0.2 g PVP and 300 μL AA into Carousel 6 Plus (100 mL). The mixture was sealed to protect it from possible oxidation, and incubated for 21 h at 90 °C under gentle stirring to attain Cu NCs@PVP.[19]

3.2.3. Protein and peptide templating. Proteins and peptides have appropriate functional groups for binding to Cu^{2+} ions, thus promoting stabilization of Cu NCs. Some proteins like bovine serum albumin (BSA) can act as both a reducing agent and a stabilizer. BSA in the presence of dithiothreitol (DTT) assisted the reduction of Cu^{2+} ions.[146] There are other additives such as H_2O_2[147] and hydrazine hydrate[13] which support such a role of BSA. In the presence of NaOH, which decomposes the BSA structure and breaks the disulfide bonds, blue emitting Cu NCs (410 nm) were produced by using BSA without any secondary reductant.[148–150] Papain is another appropriate protein that has been used as a template for the formation of Cu NCs. In the presence of hydrazine hydrate as the reducing agent, red emitting Cu NCs (620 nm) under UV excitation (370 nm) can be synthesized.[151] Lysozyme,[152] yeast,[153] and trypsin[13] are also good templates for Cu NC synthesis. Gao *et al.*[154] designed a peptide CCYGGPKKKRKVG and applied it as the template to obtain blue emitting Cu NCs (418 nm). In a similar work, a CLEDNN peptide was used as a template and AA as the reducing agent.[155] Egg white is an easily available template for the one-pot synthesis of Cu NCs. Bhamore *et al.*[72] mixed egg white with hydrazine hydrate, NaOH, and $CuSO_4$ and heated the mixture inside a microwave at 100 W for 5 min to prepare multicolor emitting Cu NCs. Similarly, Ding *et al.* and Qiano *et al.*[156,157] incubated a mixture of $CuCl_2$, chicken egg white and NaOH at 55 °C for 8 h to prepare Cu NCs as fluorescent probes.

3.2.4. Other templating methods. In addition to the aforementioned templates, there are other substances that can be used as a scaffold for the preparation of functional Cu NCs. Biosynthesis of Cu NCs with strong PL emission (500–650 nm) under 405 nm excitation by MDA-MB-231 cells in the presence of L-glutathione as the reducing agent was performed by Ye and co-workers.[73] Hu *et al.*[158] employed DTT as a template to prepare orange-florescent Cu NCs for detection of Al^{3+} ions in food samples. Biswas and co-workers synthesized Cu NCs of

diameter 1–4 nm by employing a millifluidic reactor,[159] with the reported advantage concerning lower amounts of required reagents and better control over the reaction temperature. The reason for attaining Cu NCs was the ability to separate the nucleation and growth stages. In a typical procedure, an aqueous solution of $Cu(NO_3)_2$ and *O*-[2-(3-mercaptopropionylamino)ethyl]-*O*′-methylpolyethylene glycol [MPEG] was pumped into the reactor, and a reducing agent ($NaBH_4$) was injected by another pump. Cu NCs were formed, separated, and collected under a nitrogen atmosphere.

3.3. Electrochemical synthesis

Electrochemical synthesis is a method that has widely been used to prepare various metal NPs and NCs. During the process, electrolysis of the copper anode releases Cu^{2+} ions, which are then reduced and capped at the cathode in the form of Cu NCs; by controlling the current density, the final size of NCs can easily be adjusted.[160] The advantages of this procedure are that Cu NCs can be synthesized at low current densities and without any additional ligands or surfactants. Under optimum conditions, PLQY of such "naked" Cu NCs could be as high as 13%, which favorably compares with many of Cu NCs prepared by wet chemical methods.[161] Huseyinova *et al.*[162] synthesized stable surfactant-free Cu_5 clusters with a blue PL emission (305 nm) under excitation at 224 nm. Vilar-Vidal *et al.*[161] produced highly stable ligand-free Cu_{13} NCs with a blue PL emission (410 nm) by using tetrabutylammonium nitrate as an electrolyte and showed that the number of atoms in the copper core (up to Cu_{20}) can be regulated by heating these clusters at 80 °C, followed by re-dissolution in acetonitrile. Green fluorescent Cu NCs with smaller dimensions (down to Cu_5 core atoms) have been produced by centrifugation in ethanol through a purification process.[163]

3.4. Etching methods

Chemical etching can be considered as a top-down method for the synthesis of MNCs from larger, non-luminescent NPs, often in the presence of suitable excess ligands or excess metal salts.[64] NCs can be synthesized from poly-disperse NPs through a digestive ripening or core etching mechanism. Using an etching approach for formation of Au and Ag NCs has been rather popular, while there are only a few examples in the case of Cu NC synthesis.[92] Wang and co-workers[22] added Cu^{2+} to oleyl amine (OA) and 1-octadecene (ODE) solution to prepare OA–Cu NPs. Etching of Cu NPs was performed by adding an aqueous solution of polyethyleneimine (PEI) to OA–Cu NPs in chloroform at 50 °C. In another experiment,[164] Cu^{2+} and AA (serving as both a reducing agent and a capping agent) were used to prepare Cu NPs, which were added to GSH aqueous solution to provide the etching process. The resulting Cu NCs exhibited a strong emission peak at 600 nm. Instead of using GSH for etching, other thiol ligands like cysteine[164,165] and penicillamine[164] can also be utilized. Xie *et al.*[166] reduced Cu^{2+} by $NaBH_4$ to attain Cu NPs protected by GSH, which were transferred to an organic phase through the addition of cetyltrimethylammonium bromide (CTAB), which were incubated for 24 h to obtain Cu NCs with a blue PL emission at 438 nm. Patra's group[92] synthesized red and blue emitting Cu NCs through the etching of Cu NPs by addition of a highly concentrated GSH. The as-synthesized red emitting $Cu_{34-32}(SG)_{16-13}$ NCs showed a PL peak at 625 nm with a low PLQY of 0.03%, which could be increased 36-fold *via* addition of EtOH with f_v = 90%. The as-prepared blue-emitting $Cu_{25}(SG)_{20}$ NCs showed a PLQY of 9.7%, which could be further enhanced two-fold by addition of EtOH with f_v = 75%. Deng *et al.*[100] developed a method to etch Cu NPs with ammonia (NH_3); green fluorescent Cu NCs with a PLQY of 6.6% were attained after ~15 min.

3.5. Other methods

There are few other techniques used for fabrication of Cu NCs which are somewhat hard to be classified into the above-mentioned groups. Lopez-Quintela and coworkers[167] employed the water-in-oil micro-emulsion technique to prepare blue emitting Cu NCs under UV irradiation, using Cu^{2+} as an aqueous solution, cyclohexane as an oily phase, $NaBH_4$ as a reducing agent and sodium dodecyl sulfate with isopentanol as a surfactant. Recently, Koninti *et al.*[168] synthesized Cu NCs inside the water pool of reverse micelles, which were made of sodium bis(2-ethyl-1-hexyl)-sulfosuccinate or Triton X-100 or CTAB. Quite remarkably, the stability of L-cysteine protected Cu NCs increased from 40 days in bulk water to 180 days in reverse micelles due to the protection of the as-synthesized clusters from aerial oxidation. Kawazaki *et al.*[169] employed a microwave-assisted polyol synthesis to produce oxidation resistant Cu NCs through *in situ* ethoxylation reaction of ethylene glycol, without the need for any additional ligands or surfactants. Toh *et al.*[170] embedded Cu NCs in ZnO thin films prepared by the radio frequency magnetron sputtering method to study their magnetic properties. The film deposition was carried out at 170 K[171,172] under the gas flow of Ar and He (100–200 cm^3 min^{-1}). Then, Cu NCs were formed on the ZnO film by using nanocluster beam deposition. The clusters had an average size of 8 to 10 nm while secondary phase nanoclusters (CuO and Cu_2O) were also formed. After depositing another ZnO layer on top of Cu NCs, improved ferromagnetism at RT was attained through the overlapping of the p-orbital from O contributed by ZnO and the d-orbital contributed by Cu. Stable and ligand-free Cu NCs were synthesized *via* an anti-replacement method.[173] A mixture of 3 mL of $CuCl_2$ solution (20 mg mL^{-1}) and 2 mL of Au NP solution (0.01 mg mL^{-1}) was irradiated by a pulse laser (532 nm) for 5 min; Cu NCs with 2.0 ± 0.4 nm diameter were formed as a result and were separated by centrifugation, and they emitted at 440 nm under 350 nm excitation wavelength. The formation mechanism of Cu NCs under laser irradiation was ascribed to the generation of "hot electrons" in Au NPs, which consequently reduced adjacent Cu^{2+} ions.

4. Applications of Cu NCs

4.1. Catalysis

Metal NCs have become quite important from the point of view of their catalytic activity, due to their ultrasmall size and high surface energy,[174,175] which capitalized on the previously conducted catalytic related studies of larger MNCs.[140] Although NCs based on

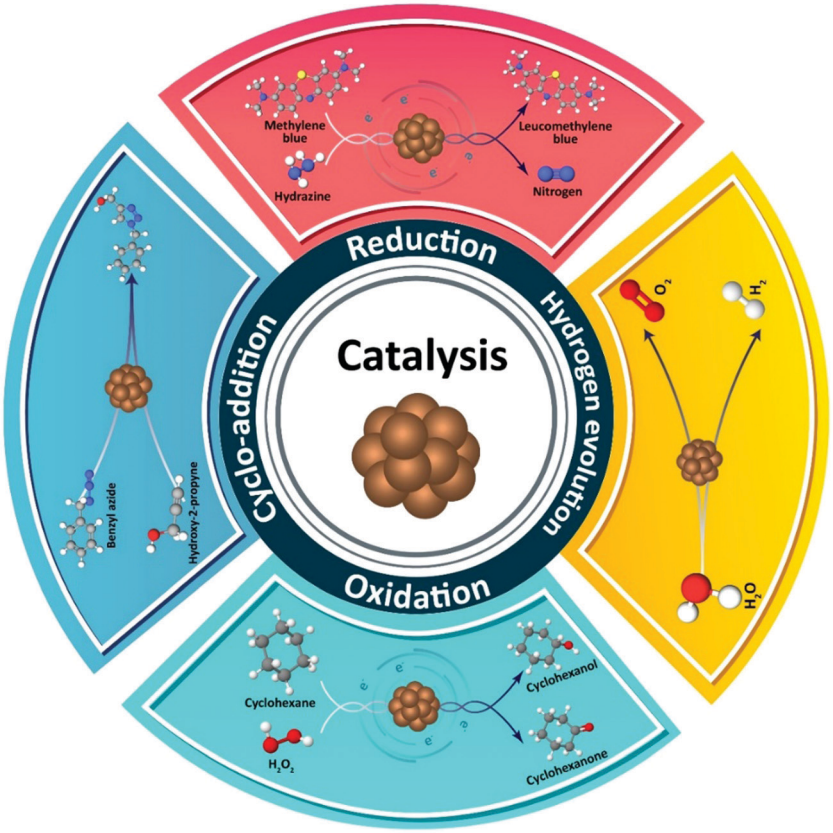

Scheme 2 Schematic representation of four different types of chemical reactions which can be catalyzed by Cu NCs.

noble metals display good catalytic performance, it is highly desirable to offer alternative, less expensive while catalytically active Cu NC analogues. Computational aided methods can suggest suitable strategies for developing active catalysts based on Cu NCs.[104] In that respect, theoretical studies on the surface chemistry of Cu NCs aimed at the exploration of adsorption steps of different chemical compounds are helpful in the understanding of various types of possible catalytic reactions. For instance, theoretical comparisons between adsorption of CO and H_2 molecules on Cu NCs by molecular dynamics simulations have shown that CO is adsorbed more easily than H_2, and this has a greater impact on the cluster structure.[176] As depicted in Scheme 2, catalytic reactions which have been performed so far on Cu NCs can be classified into four groups, including reduction, oxidation, hydrogen evolution reaction (HER), and 1,3-dipolar cycloaddition. Examples of Cu NCs used in these kinds of catalytic reactions are outlined below and listed in Table 1.

4.1.1. Reduction. Methylene blue (MB) can be reduced to lucomethylene blue by using hydrazine as a reducing agent. Kinetic studies have shown that in the absence of Cu_{13} NCs, the optical density of MB was not changed during the reaction; however, in the presence of electrochemically synthesized Cu_{13} NCs, a fast reduction occurred, and the Cu NCs retained their catalytic activity for at least 42 cycles.[140] It was also shown that the increase of concentration of Cu_{13} NCs and hydrazine resulted in the enhancement of the rate constant, while the reaction became slower in acidic solutions. It was noted that the size of Cu NCs is very crucial because larger clusters (*e.g.* Cu_{20} NCs) have not exhibited catalytic activity for this reaction.[140]

Titanium dioxide is a very well-known photocatalyst that has attracted researchers' attention in the last decades. To improve visible light sensitivity of TiO_2, Liu *et al.*[177] prepared Cu(II) NC-grafted Nb-doped TiO_2. Nb ions reduced the energy level below the conduction band of TiO_2 to be matched with the $E_{Cu^{2+}/Cu^{+}}$ (redox potential) of the Cu(II) NC complex on the surface of the catalyst. The resulting Cu(II)–$Nb_xTi_{1-x}O_2$ nanocomposite could decompose 2-propanol as an organic compound into CO_2 under visible light. A theoretical and experimental study demonstrated that deposition of Cu_5 NCs on the surface of TiO_2 NPs could extend visible light absorption and lead to the formation of an efficient photocatalyst.[178]

Cai *et al.*[15] deposited bimetallic Cu/Au NC catalysts onto a MgO powder support for the reduction of 4-NP to 4-AP by $NaBH_4$. Cu-rich NCs, Au-rich NCs or Cu/Au-equal NCs formed an alloy structure randomly. The reaction rate constant of 3.49×10^4 min^{-1} mole of $metal^{-1}$ was attained from the Cu/Au-equal NC catalyst, which was 6.6 (8.9) fold higher than that for the Cu-rich (Au-rich) NCs. Theoretical modeling determined the balancing of the adsorption of 4-NP and desorption of 4-AP, which enhanced the activity of Cu/Au-NC catalysts. It was also found that the activity of Cu/Au-equal NCs prepared by beam

deposition was 25 fold higher than that of the catalyst synthesized by wet chemistry.

The first report on the catalytic activity of copper-based structures for reduction of CO_2 appeared in 1981.[179] Tang and co-workers[180] utilized $Cu_{32}H_{20}L_{12}$ NCs (L is dithiophosphate ligand) to reduce CO_2 to CO and HCOOH. After adsorption of CO_2 on the surface of the catalyst, the main step was where the hydrogen was added: combination of hydrogen with C would facilitate the reaction to form HCOOH, while addition of hydrogen to O would produce CO. The turnover number of $Cu_{13}H_{20}L_{12}$ NCs has been determined as ~1740 mole HCOOH per mole of $Cu_{32}H_{20}L_{12}$.

Although use of the thiolate ligands may become detrimental for achieving high catalytic activity, there have been reports on thiolated Cu NCs showing decent catalytic performance.[181] Based on the density functional theory (DFT) simulations, thiolated $[Cu_{25}H_{10}(SPhCl_2)_{18}]^{3-}$ NCs were introduced as a catalyst for reduction of ketones to alcohols in the presence of hydrogen at RT.[182] Other studies suggested that the migration of ligands and their partial removal activate catalytic performance of thiolated metal NCs.[183,184]

Even though Au NCs are most popular for electrochemical reduction,[185] several studies[96,186] have shown that Ag and Cu NCs are also electro-catalytically active. It was reported that Cu_n ($n < 9$) NCs have high catalytic activity for the oxygen reduction reaction (ORR).[187] Results of electrochemical cyclic voltammetry (CV) also indicated that Cu NCs with smaller core sizes exhibited higher electro-catalytic activity for oxygen reduction.[96,188] Ligand-free Cu NCs were introduced as electrocatalysts for the ORR.[173] Reduction currents were observed when Cu NCs were immersed in 0.1 M KOH solution saturated with either O_2 or N_2, with respective current density 22 and 1500 times higher than that of Au NCs and protected Cu NCs of similar size (Fig. 3A). The mass activity of these Cu NCs was 1.6 and 4.2 fold higher than that of the target set by the U.S. Department of Energy and the commercial Pt catalyst. Such a high electrocatalytic activity was ascribed to the clean surface in the absence of ligands, which greatly facilitated the electron transfer. Interestingly, ligand-free Cu NCs were also quite durable: The current–time response of Cu NCs retained 88.1% of its initial value after 10 000 s (Fig. 3A), which was better than that for the ligand-functionalized Cu NCs used for comparison.

By employing DFT, the effect of chalcogen (oxygen family elements) doping on the catalytic activity of Cu_4 NCs was systemically investigated.[189] Doped Cu NCs could electrochemically reduce CO_2 to CH_4 and CH_3OH. It was also shown that the activation energy barrier for CO_2 hydrogenation to CH_4 was reduced by Cu_4S and Cu_4O NCs by 0.15 eV and 0.37 eV, respectively, and over-potentials for the reaction changed in the order of $Cu_4S < Cu_4O < Cu_4Se$.

4.1.2. Oxidation. Wang *et al.*[13] employed BSA–Cu NCs as a catalyst for styrene oxidation. They showed that in the presence of this catalyst, 70% of styrene was converted to products with high selectivity (70% of products was benzaldehyde), while without the catalyst only 7% of styrene could be converted. Takahashi *et al.*[190] used $Cu_{32}Pt_{16}Au_{12}$ multi-metallic nanoclusters (MNCs) for the oxidation of indane to indanone in an oxygen atmosphere (1 atm). It was shown that the catalytic activity of MNCs was 24 times higher than that of commercial Pt catalysts and 5 times higher than that of Pd–Au. The turn over frequency (TOF) for this catalyst was 1433 (total metal atom^{-1} hour^{-1}) at 90 °C under pure oxygen. They also claimed that MNC catalysts could be utilized for other compounds with primary C–H bonds, like xylene. He *et al*[191] suggested soluble Cu NCs as an alternative for alkaline metal alkoxide catalysts in the industrial carbonylation reactions. The high activity of Cu NCs for green oxidation of methanol to methyl formate with CO was demonstrated, and complete conversion into this compound under controlled reaction conditions (0.3–3.0 MPa CO, 353–443 K) was shown.

Sarkar and co-workers[17] synthesized Cu NCs supported on Cr_2O_3 for the oxidation of cyclohexane. Cr_2O_3–4.4wt% Cu showed the highest selectivity and conversion in comparison to CuO,

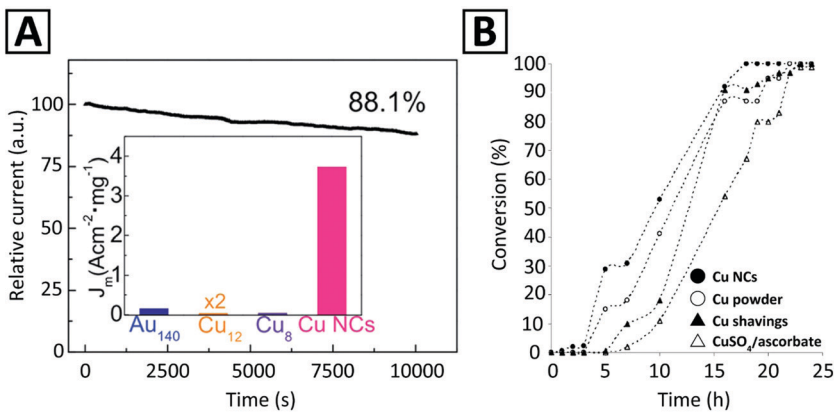

Fig. 3 (A) Time-dependent reduction current (in the O_2-saturated solution, at 0.9 V) of ligand-free Cu NCs used as an electrocatalyst for the ORR. The inset compares the current density (J_m) per mass unit of the ligand-free Cu NCs with that of several ligand-functionalized MNCs, namely, $Au_{140}(S(CH_2)_5CH_3)_{53}$, $Cu_{12}DT_8Ac_4$, and $Cu_8(C_7H_9N_2S)_4$. Adapted with permission from ref. 173, Copyright 2018, RSC. (B) Observation of time-dependent conversion profiles for the 1,3-cycloaddition of prop-2-yn-1-ol to benzyl azide employing different Cu catalysts. Adapted with permission from ref. 11, Copyright 2005, Wiley-VCH.

Cu_2O, and other proportions of Cu–Cr_2O_3 catalysts. This catalyst exhibited 86% conversion to cyclohexanone and cyclohexanol, with 85% selectivity of formation of cyclohexanone, and its TOF was about 52.5 and did not change after 4 successive runs. In another study, a 0.9%Cu/SiO_2–MnO_2 catalyst for oxydehydration of glycerol was used,[192] with the main products being acrylic acid and acrolein. The conversion efficiency of glycerol was 77.1%, while the attained acrylic acid selectivity was 74.7%, and the TOF for this catalyst was 32.9 h^{-1}. Commercial MnO_2 showed only 5.5% conversion of glycerol under the same conditions. Athawale and Bhagwat[193] used a Cu NCs/polyaniline composite as a catalyst for a Wacker oxidation reaction, where 1-decene was converted into 2-decanone in the presence of molecular oxygen. Hu *et al.*[194] showed that 3,3′,5,5′-tetramethylbenzidine could be oxidized by H_2O_2 in the presence of Cu NCs; the reaction would not proceed without a catalyst. In a theoretical study, Tang *et al.*[195] investigated the catalytic action of Cu_{55} NCs on the oxidation of CO to CO_2. It was found that the oxidation process is catalyzed by Cu NCs through two mechanisms: Eley–Rideal (adsorption of oxygen molecules on the cluster surface and then interaction with CO) and Langmuir–Hinshelwood (co-adsorption of O_2 and CO).

4.1.3. Hydrogen evolution reactions and hydrogen dissociation. Hydrogen is considered as a biofriendly fuel gas, and has the largest energy density; therefore, hydrogen evolution reactions (HER) are important in the renewable energy industry. Tang and co-workers[180] used $Cu_{32}H_{20}L_{12}$ NCs for the reduction of CO_2, as we already discussed above. The HER may occur in competition of the reduction reaction according to $Cu_{32}H_{20} + H^+ + e^- \rightarrow Cu_{32}H_{19} + H_2$ (Heyrovsky mechanism), or $Cu_{32}H_{19} + H^+ + e^- \rightarrow Cu_{32}H_{20}$ (Volmer reaction). At high over-potential, the HER is preferable while at low overpotentials the formation of HCOOH is more susceptible. Recently, $[Cu_{32}(H)_{20}\{S_2P(O_2Bu)_2\}_{12}]$ and $[Cu_{20}H_{11}\{S_2P(O_2Bu)_2\}_9]$ have been introduced;[196] although the high molecular weight of supporting S-based ligands utilized in the stabilization of these Cu NCs did not make them good candidates for H_2 storage, they offered a platform to release H_2 under extremely mild conditions, which could qualify metal hydrides to become exceptional models for the HER, such as those able to harvest solar energy.

The densest crystallographic plane of copper with the lowest surface energy is the (111) plane.[197] This surface plane can become unstable under CO exposure (0.1 to 100 Torr) at RT to form Cu NCs, with the edge of Cu atoms decorated by CO molecules.[16] DFT simulations have shown that the energy of CO binding to low-coordinated Cu atoms and the weakening of binding of Cu to neighboring atoms drive this process. Cu NC formation could activate the surface for the water dissociation reaction (*e.g.* $CO + H_2O \leftrightarrow CO_2 + H_2$) leading to the production of H_2. It is noteworthy that no clustering was detected on the surface of Pt(111) under CO exposure.[16] Even though the high surface area of Cu NCs provides high catalytic selectivity, its kinetic rate for H_2 dissociation is very low.[198] Very recently, Hoyt *et al.*[104] employed DFT to explore the mechanism of how Cu NCs improve the catalytic activity for the HER. They showed that an icosahedral Cu_{13} NC has a large magnetic moment, which influences the catalytic behavior. The most capable transition state for H_2 dissociation has lower energy of activation than that of single-crystal Cu surfaces, but needs a magnetization change from 5 to 3 μ_B. Fragile spin–orbit coupling delays this change, reducing the kinetic rate of H_2 dissociation by a factor of 16. Strategies to aid magnetization change through environmental magnetic stimulus can improve the catalytic efficiency of Cu NCs.

4.1.4. 1,3-Dipolar cycloaddition. 1,3-Dipolar cycloaddition is a chemical reaction between a 1,3-dipole and a dipolarophile to form five-membered heterocycles and their ring-opened acyclic derivatives, which is sometimes referred to as Huisgen cycloaddition. While this reaction generally does not proceed readily under mild conditions, Cu(I)-catalysts have been able to accomplish it even under physiological conditions (neutral pH, RT and water solution).[199] Only a few examples are documented in the literature on using Cu NCs for this reaction. Lee *et al.*[11,200] developed a hydride-centered dithiophosphate cluster ($[Cu_8(\mu_4\text{-}H)\{S_2P(OEt)_2\}_6](PF_6)$) which was able to catalyze the 1,3-dipolar cycloaddition of organic azides and alkynes into substituted triazoles. The required catalyst loading was as low as 0.4 mole%. The formation of the obligatory Cu(I) acetylide intermediate was suggested to be facilitated by the abstraction of the terminal hydrogen of alkynes by the hydride released from the central part of the cluster. Pachón *et al.*[11,200] have demonstrated that air-stable Cu NCs are good candidates for the Cu(I)-catalysed "click" cycloaddition of azides. Monitoring the reaction kinetics between prop-2-yn-1-ol and benzyl azide, conversion profiles were obtained for 4 different catalysts, including Cu NCs, Cu powder, Cu shavings, and $CuSO_4$/ascorbate (Fig. 3B). Significant differences in the reaction kinetics were observed, and it was noted that Cu NCs did not serve as a Cu(I) reservoir. Cu NCs showed the highest activity among the 4 catalysts studied, and achieved 100% conversion after 18 h (Fig. 3B).

Other studies suggested that organometallic Cu NCs are more active than thiolated ones.[12] The catalytic activity of $[Cu_{20}(CCPh)_{12}(OAc)_6]$, both in a bare form and immobilized on silica, in the Huisgen cycloaddition was examined. Unsupported Cu NCs used as a homogeneous catalyst were unstable and dissociated into smaller NCs and/or discrete Cu(I) cations; on the other hand, silica-supported Cu NCs displayed comparable yields even after recycling.

4.2. Sensing

Cu NCs have been widely applied in sensing using several strategies, including electrochemical signaling, enzyme mimetic activity, and optical responses. Among these sensing schemes, the detection based on absorption and emission properties has been employed more frequently, and included *in situ* synthesis of fluorescent Cu NCs (through the turn on/turn-off mechanism), fluorescent quenching through the inner filter effect (IFE), FRET, and electron transfer, and enhanced fluorescent intensity (mostly due to AIE mechanisms). Accordingly, a lot of studies have recently been conducted on potential applications of Cu NCs as a fluorescent sensor for detection of various compounds such as anions, namely, halides (Cl^-, Br^- and I^-),[63,201] S^{2-},[28,153,165,202,203] NO_2^-,[65,131] CN^-,[65] $Cr_2O_7^{2-}$,[64] and phosphate;[204] cations, such as Ag^+,[63,205]

Hg^{2+},[38,62,147,206,207] Al^{3+},[61,158,208] Zn^{2+},[208,209] Fe^{3+},[4,30,108,138,210–213] Au^{3+},[214] Mn^{2+},[133] Pb^{+},[215] chromium(IV),[216] Cr^{6+},[217] Cu^{2+};[218–220] various organic compounds; water in organic solvents;[60,221] and H_2O_2[9,117,126,137] and H_2S[156,222,223] in aqueous systems. Regarding organic compounds, Cu NC based sensors have been applied for detection of various medications including tramadol,[26] methotrexate,[51] carbamazepine,[52] nitrofurantoin,[42] *o*-phenylenediamine,[224] doxycycline,[25] and tetracycline;[225] biocidal and herbicidal compounds such as thiram and paraquat;[72] explosive compounds including trinitrotoluene (TNT),[71,226,227] *m*-dinitrobenzene,[55] nitrofurantoin,[34] RDX,[27] and trinitrophenol (TNP);[19,228] food additives such as melamine,[229] folic acid,[56] quinoline yellow,[224] gossypol;[29] humidity and ethanol.[59] Representative examples are presented in Table 1 and are briefly outlined below.

4.2.1. Organic molecule sensing. Several characteristics of Cu NCs such as cost-effectiveness, biocompatibility, and attractive emission properties make them promising candidates for detection and quantification of several medications in biological fluids, such as doxycycline, tramadol, carbamazepine, methotrexate, nitrofurantoin (NFT), and so on. Compared with other methods such as capillary electrophoresis, chromatography, ion mobility measurements and electrochemical methods, luminescence-based techniques are simpler, more cost-effective, and highly sensitive for detection of biomolecules. Recently, a high-performance chemiluminescence technique was reported for sensitive quantification of tramadol within a linear concentration range of 0.003–2.5 μM and a limit of detection (LOD) of 0.8 nM using BSA–Cu NCs encapsulated into the nanoporous structure of a flake-like copper-based MOF as a support material. To improve the selectivity toward tramadol, a pre-extraction step has been applied using MIP-Fe_3O_4@SiO_2 nanoparticles in a dispersive solid phase extraction method.[26] Fluorescent bimetallic NCs composed of copper and other metals such as Pd, Au, Ag, and Mo have also been developed. A fluorescence sensor based on Cu/Mo bimetallic NCs with a PLQY of 26% has been used for detection of methotrexate, an anti-neoplastic drug, within a linear range of 50 nM to 100 μM and LOD of 13.7 nM.[230] CTAB-coated Cu NCs were employed for detecting carbamazepine in exhaled breath condensate within a linear range of 0.2 to 20 μg mL^{-1} and LOD of 0.08 μg mL^{-1}.[52]

Orange-fluorescent Cu NCs (560 nm) with a PLQY of 5.8% were synthesized using ovalbumin and applied for detecting doxycycline with a linear range from 1 to 1000 μM, and LOD of 270 nM.[25] This sensing probe was also applicable for detecting doxycycline in urine specimens as a real sample with recoveries over 90%. In the presence of doxycycline, Cu NCs@OVA exhibited a high PL enhancement due to the interaction between doxycycline and ovalbumin that results in the formation of a more compact structure of the nanoclusters. Under UV excitation, a change in the solution color containing a different concentration of doxycycline (from orange to yellow) occurred. Additionally, Cu NCs@OVA showed high selectivity for doxycycline detection compared with other antibiotics such as penicillin, ampicillin, streptomycin, lincomycin, and norfloxacin. It was emphasized that the aqueous solubility of these clusters provided by multiple hydroxyl groups on the surface as well as their low toxicity and biocompatibility features could make them suitable for *in vivo* applications.[25,72] They also exhibited good stability in hyper-saline environments (at 40 °C and under photobleaching conditions) and in the presence of several organic solvents and metal ions.[25]

A label-free, "turn off" analytical strategy using water-soluble adenosine-stabilized Cu NCs has been developed by Wang *et al.*[34] This fluorescent sensing probe showed fast, sensitive and selective response to nitrofurantoin (NFT) in a wide linear range of 0.05–4.0 μM with a detection limit of 30 Nm, and has been used for the analysis of lake water samples with a recovery of 96–105% and relative standard deviation lower than 2%. The emission intensity of the adenosine-stabilized Cu NCs reduced with a gradual shift towards longer wavelengths at higher NFT concentrations. A small variation in the PL spectra of Cu NCs in the presence of many other substances such as phenylalanine, proline, isoleucine, valine, alanine, glutamic acid, serine, glycine, lysine, leucine, glutamine, methionine, tyrosine, aspartic acid, asparagine, threonine, arginine, cysteine, glucose, and uric acid (at 1.0 μM) proved the high selectivity of this probe to NFT. The quenching mechanism has been proposed to be based on the IFE between adenosine-stabilized Cu NCs and NFT, because of the overlap between the absorption band of NFT at 250–430 nm and the excitation and emission of Cu NCs. A ratiometric sensor based on GSH-stabilized Cu NCs for the detection of o-phenylenediamine (OPD), as an intermediate in medicine production, has been developed, and exhibited a linear detection range of 0.15 to 110 μg L^{-1} and LOD of 93 ng L^{-1}. In the samples of river water and textile dyeing wastewater, its recovery rate was 96.8% and 100.3%, respectively.[224]

Quantitative detection of explosive compounds such as nitroaromatics (*e.g.* trinitrophenol, dinitrobenzene, TNT) and heterocyclic nitramines (*e.g.* trinitrotriazine, RDX) using Cu NCs as a turn-on/turn-off luminescent probe has been reported. Cysteine-stabilized Cu NCs were employed for selective sensing of dinitrobenzene and picric acid based on a turn-on fluorescence mechanism.[55] The sensor exhibited a linear range of 99 nM to 1.3 and LOD of 0.13 μM. Quantitative detection of RDX with a LOD of 1.62 nM in a linear concentration range of 0 μM to 0.238 μM was performed using BSA-stabilized Cu NCs;[27] it was based on the turn off–on fluorescence mechanism using Zn^{2+} ions as a modulator. Upon adding RDX, due to the Lewis acid–base interactions between Zn^{2+} and trinitrotriazine, fast recovery of Zn^{2+} induced fluorescence quenching of Cu NCs was realized. A TNT probe based on L-cysteine modified Cu NCs with a LOD of 9.1 nM,[71] and a luminescence sensor using a Cu NCs-ZIF-8 nanocomposite with a LOD of 8.5 μM[227] have been demonstrated. Recently, a fluorescent and colorimetric sensor for selective and sensitive detection of trace amounts of TNT both in solution (LOD = 14 pM) and in the gas phase (LOD = 0.05 nM) based on water-soluble PEI-capped Cu NCs has been developed.[18] Their high sensitivity arises from selective binding between PEI and an electron deficient molecule such as TNT; it can result in a charge transfer complexing interaction between the aromatic ring of TNT and amino groups of PEI-capped Cu NCs through a photo-induced electron transfer (PET) reaction. In the presence of TNT, the emission of

NCs was quenched, which could be related to the formation of a Meisenheimer complex through acid base pairing, hydrogen bonding, and electrostatic interactions. The selective sensing performance of the PEI-capped Cu NCs compared with some organic molecules such as toluene, nitrobenzene (NB), 4-nitrotoluene (4-NT), trinitrophenol (TNP), dinitrophenol (DNP), RDX and 4-nitrophenol (4-NP) could arise from the absence of the Meisenheimer complex. Preparing paper strips of PEI-capped Cu NCs with storage stability over one month has also been reported, which could be useful for rapid onsite and visual detection of TNT.[18] These paper strips showed a detection limit of 10 nM within 1 min for sensing of TNT in vapor form. Green fluorescent PVP-stabilized Cu NCs with a large Stokes shift and a high PLQY (>44%) were used for detection of trinitrophenol (TNP) with a LOD of 0.391 μM.[19]

A chemiluminescent sensor based on L-Cys stabilized Cu NCs-DPA was developed for the detection of folic acid with a linear concentration range of 0.1–10 μM and LOD of 69.8 nM. A similar sensor based on Cu NCs–DPA–FA was used for detection of nitrites, and exhibited a linear range of detection within 0.1–80.0 μM and LOD of 0.0954 μM.[56] Blue emitting L-Cys stabilized Cu NCs were used for detection of quinoline yellow as a food colorant, with a linear concentration range from 0.2 to 5.5 μM (LOD of 0.11 μM) and high selectivity compared with other yellow colorant additives such as sunset yellow and tartrazine.[224] Formation of a stable complex between gossypol and BSA in a BSA–Cu NCs has been used in a fluorescence-based probe for detection of gossypol, with a linear range of 0.1–100 μM and LOD of 25 nM. This sensor was used in real samples (cottonseed meal and oil), and exhibited a selective fluorescent quenching behavior in the presence of interfering compounds such as Na^+, K^+, Ca^{2+}, Mg^{2+}, Zn^{2+}, glucose, glycine, and palmitic acid.[29]

4.2.2. H_2O and H_2O_2 sensing. A dual-emitting film composed of GSH–Cu NCs and carbon dots (CDs) has been used by Wen *et al.*[59] for the detection of atmospheric humidity in the range of 40–80%. The sensor was prepared through the infiltration of a CD solution in a filter paper followed by dipping in a Cu NC solution and then drying under vacuum. An increase in the air humidity induced a color change of the film from red to blue; it could also be used for simultaneous detection of ethanol and water. A nanoswitch of copper nanoclusters (AMTD–Ac–Cu NCs) stabilized by dual ligands 2-amino-5-mercapto-1,3,4-thiadiazol (AMTD) and acetate (Ac-) has been developed by Cheng *et al.*[60] for sensitive detection of trace water in organic phases. It operated in a reversible way between two states including ''fluorescence off'' in the solid form and ''fluorescence on'' in the presence of water, where the strong hydrogen bonding between water and AMTD/Ac resulted in the aggregation of Cu NCs. High sensitivity, good reversibility, and a repeatable response have been reported for water sensing with the maximum fluorescence intensity for the water content of 50.0%, 35.48%, 35.48%, and 39.39% (MeCN) in EtOH, THF, ACT, and MeCN solvents, respectively. The detection limit was 0.036 for EtOH, 0.018 for THF, 0.024 for ACT, and 0.026 for MeCN. Time-resolved luminescence decay curves exhibited a long lifetime of 3.14 ns, which indicated a type of phosphorescence behavior. Importantly, aqueous solutions of these Cu NCs had long-term stability for several months.

Detection of H_2O_2 in aqueous solutions in a concentration range from 1 μM to 1 M by a direct and fast colorimetric sensing probe and without using any chromogenic reagent or expensive instrument has been reported by Du *et al.*[117] The sensing probe has been prepared using water-soluble mercaptosuccinic acid stabilized Cu NCs (MSA-capped Cu NCs). The color of a diluted Cu NC solution exhibited a change from claret-red at low concentrations of H_2O_2 (about 0.001 mM) to saffron yellow at high concentrations (about 1000 mM) (Fig. 4A-I). With increasing concentration of H_2O_2 from 0 to 1 mM, the absorption peak at 520 nm was gradually quenched due to the aggregation and growth of Cu NPs *via* the cleavage of Cu–S bonds and detachment of MSA from the Cu NP surface (Fig. 4A-II). By a further increase in the H_2O_2 concentration from 1 mM to 1000 mM, the absorption peak at 375 nm was progressively increased because of Cu_2O formation (Fig. 4A-III). Therefore, the MSA-capped Cu NCs could be applied as a colorimetric H_2O_2 sensor in a wide range of 0.001 mM to 1000 mM. These Cu NCs also revealed a desirable selectivity and salt tolerance capability for H_2O_2 sensing in real water samples with recoveries in the range of 96.7% to 104.1% and a relative standard deviation lower than 4%. They also demonstrated a fast kinetics reaction of about 60 s, a slight influence of temperature (20–40 °C) on the absorption response, and storage stability of the purified and freeze-dried Cu NCs for 10 months (under dark conditions).

4.2.3. Ion sensing. Trace detection of heavy metal ions such as Hg^{2+}, Pb^{2+}, Cr^{6+}, and Cr^{3+} based on Cu NCs has been extensively reported in the literature. Bi-ligand stabilized Cu NCs composed of thiosalicylic acid and cysteamine at different ratios showed a PLQY of up to 34% and were used for Cr^{+6} detection in a linear range of 0.1–1000 μM with a LOD of 0.03 μM.[217] The PL quenching in the presence of Cr^{6+} ions was related to the IFE mechanism because of a large overlap between the Cu NC excitation and Cr^{6+} absorption spectrum. In a real sample examination (mineral water), a high recovery in the range of 98.3–105.0% was attained. Li *et al.*[38] presented a sensor based on reticular DNA templated–Cu NCs aggregates for sensitive and selective detection of Hg^{2+} in real water samples (lake water), with high recovery (98 to102%) and low relative standard deviation (1.6–4.6%). The rigid nature of the reticular DNA as a template led to the formation of Cu NC aggregates with greatly enhanced emission compared with single-stranded DNA-templated Cu NCs. The dual-function of DNA manipulation including Hg^{2+} induced fluorescence enhancement and Hg^{2+}-induced enzyme restraint resulted in the fabrication of a Hg^{2+} biosensor with a remarkably enlarged signal-to-noise ratio (from 2.2 to 56.1), which made it possible to quantify Hg^{2+} in the range of 50 pM up to 500 μM with an ultra-low detection limit of 16 pM (Fig. 4B). Due to the specificity of T-Hg^{2+} interaction, the fluorescence intensity at 650 nm was not significantly affected by replacing Hg^{2+} with other metal ions such as Na^+, K^+, Li^+, Mg^{2+}, Ca^{2+}, Co^{2+}, Ba^{2+} and Ni^{2+} ions, which indicated the selectivity of the sensor. Bhamore *et al.*[62] used Curcuma root extract

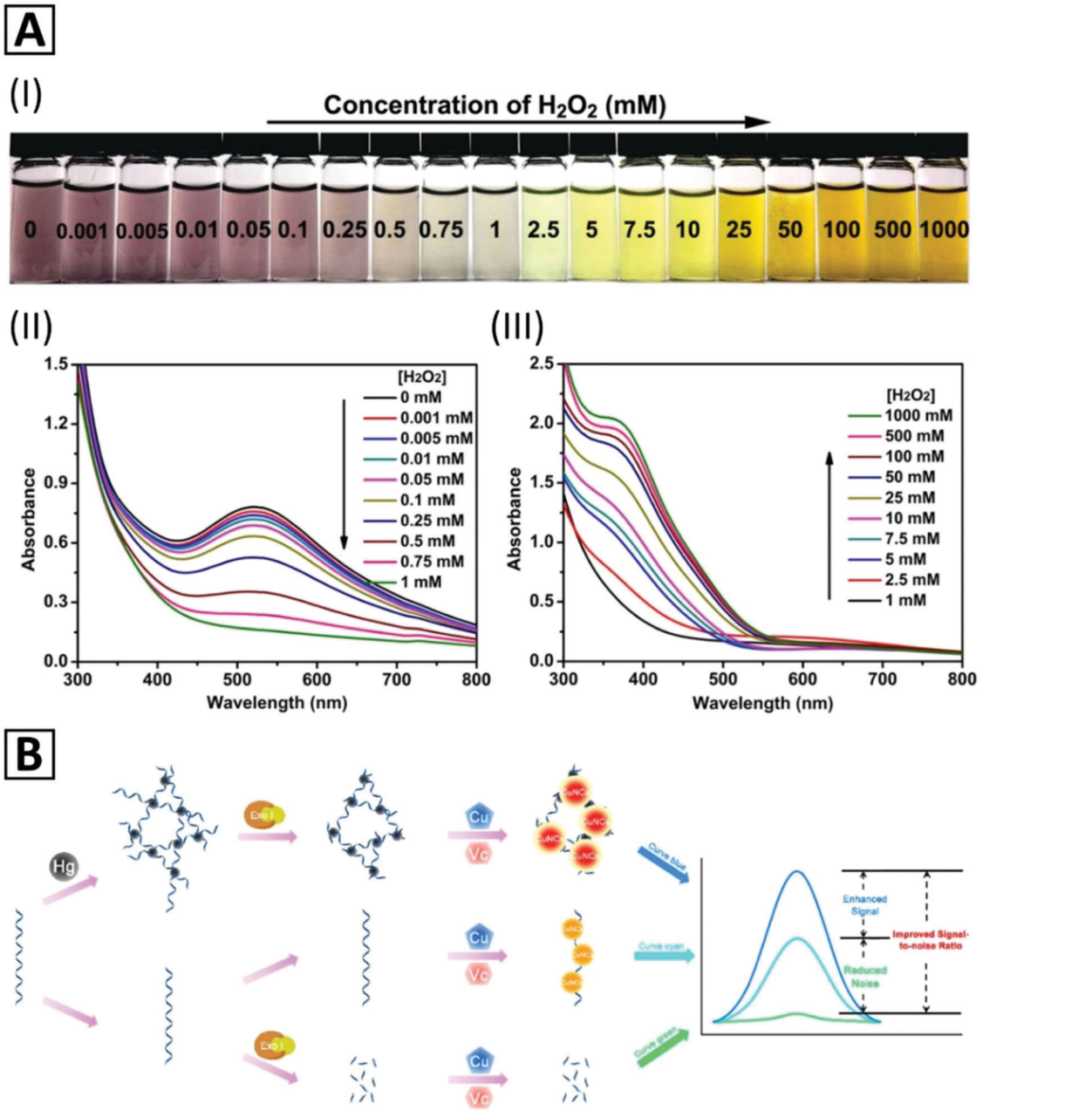

Fig. 4 (A) Color change of PBS solution (pH = 7.4, 10 mM, 37 °C) containing MSA-capped Cu NCs with the addition of H_2O_2 of different concentrations (I); UV-Vis absorption spectra of the MSA-capped Cu NCs in the presence of H_2O_2 with concentrations of (II) 0.001 mM to 5 mM and (III) 5 mM to 1000 mM. Adapted with permission from ref. 117, Copyright 2017, ACS. (B) Schematic representation of a Hg^{2+} biosensor based on reticular DNA templated–Cu NC aggregates. Adapted with permission from ref. 38, Copyright 2018, ACS.

templated–Cu NCs with a PLQY of 7.2% for detecting Hg^{2+}, with a LOD of 0.12 nM and a linear range of 0.0005–25 μM. Liu *et al.*[232] presented metallothionein-stabilized Cu NCs for visual detection of heavy metal ions. The colorimetric sensor utilized the effect of Hg^{2+} and Pb^{2+} on the enzyme-like activity of MT–Cu NCs *via* changing it from the catalase-like activity to the peroxidase-like one. The linear range of detection for Pb^{2+} was 0.7–96 μM, and for Hg^{2+} it was 97 nM–2.3 μM and 3.1–15.6 μM. LODs were 142 nM and 43.8 nM for Pb^{2+} and Hg^{2+}, respectively.

A fluorescent chemodosimeter for sensitive and selective detection of Al^{3+} in real water samples with a recovery of 92–101% and a relative standard deviation of less than 4% has been reported by Boonmee *et al.*[61] using cysteamine–Cu NCs as a sensing probe. This sensor worked in a concentration range of 1–7 μM with a low detection limit of 26.7 nM. The Cu NCs were synthesized by a ligand-assisted method in which cysteamine (Cys), a weak base containing $-NH_2$ and –SH moieties, was applied as both a capping agent and a reducing agent. The –SH moiety attached to the surface of Cu NCs through

Cu–S bonding, and the $–NH_2$ moiety acted as a receptor interacting with metal ions through different interactions such as electrostatic interactions under acidic conditions. Al^{3+} ions could interact with $–NH_2$ moieties on the surface of Cu NCs resulting in the aggregation of the NCs and subsequently an enhancement of the fluorescence intensity depending on the concentration of Al^{3+}. According to the aggregation-induced emission (AIE) mechanism, the fluorescent intensity of Cys–Cu NCs at 380 nm linearly increased with Al^{3+} concentration.

D-Penicillamine capped-bimetallic AuCu NCs have been used as a fluorescent probe for Fe^{3+} detection in rain and river water, as well as in human blood serum.[213] A high selectivity in the presence of various anions and cations especially Fe^{2+} has been demonstrated. Quenching of the PL intensity in the presence of Fe ions occurred through the IFE mechanism because of the overlap between the Fe^{3+} absorption peak and excitation peak of bimetallic AuCu NCs located at around 275 nm. The sensor exhibited a linear detection range of 0.5–7.0 μM and 7.0 μM–0.1 mM, and a LOD of 0.1 μM. Synthesis of water-soluble L-histidine-capped Cu NCs, stable against photobleaching and with long-term storage stability for sensitive and selective detection of Fe^{3+} has been performed by Lin *et al.*[210] The LOD of this sensor was 82 nM in a concentration range of 0.10 to 20 μM. High quenching efficiency and stable sensing conditions were achieved at pH = 4.1. The sensing mechanism was based on a fluorescence ''turn off–on'' mechanism in which the fluorescence intensity of the L-His–Cu NCs was quenched due to the aggregation of the particles through bonding between Fe^{3+} ions with amine groups of L-histidine. The fluorescence intensity increased after adding ethylenediaminetetraacetate (EDTA) into the mixture of L-His–Cu NPs with Fe^{3+}. This chemosensor was employed to detect Fe^{3+} in real water samples, including tap water and river water with recoveries in the range of 82.8–107.4%. L-Histidine-capped Cu CNs exhibited a selective sensing performance towards Fe^{3+} compared with various interfering ions such as Na^+, K^+, Li^+, Ca^{2+}, Mg^{2+}, Co^{2+}, Ni^{2+}, Pb^{2+}, Zn^{2+}, Mn^{2+}, Cu^{2+}, Hg^{2+}, Cd^{2+}, Al^{3+}, and Fe^{2+}, as well as some common anions such as F^-, Cl^-, Br^-, I^-, Ac^-, $NO_3{}^{2-}$, $PO_4{}^{3-}$, $CO_3{}^{2-}$, $SO_4{}^{2-}$, and $SO_3{}^{2-}$.

A turn-on PL sensor based on silk fibroin (SF) protected–Cu NCs (SF@Cu NCs) has been developed by Zhang *et al.*[203] It was used to detect S^{2-} in aqueous solutions with a LOD of ~0.3 μM and a linear range of 5–110 μM. The working mechanism of the sensor was ascribed to the assembly induced emission enhancement (AIEE). In the presence of S^{2-} ions, SF@Cu NCs aggregated to larger, rod-shaped nanoparticles, which led to an increase of the PLQY from 1.6% to 4.9%. High selectivity was observed towards S^{2-} in the presence of different interfering ions and macromolecules, and in particular sulfur-containing ions such as $SO_3{}^{2-}$, $SO_4{}^{2-}$, $S_2O_4{}^{2-}$ and SCN^-. A DNA templated–Cu/Ag NC fluorescent probe was developed by Ding *et al.*[156] to detect S^{2-} with a LOD of 3.75 pM and a wide linear concentration range from 10 pM to1 mM. This sensor worked due to the PL quenching of DNA–Cu/Ag NCs in the presence of sulfide; application for measuring sulfide amount in mouse blood (H_2S poisoned blood sample) was demonstrated. Sulfide ion detection using water-soluble Zn-modified Cu NCs based on a protein/peptide templated method has been reported by Li *et al.*[202] As compared with bare Cu NCs, Zn-modified Cu NCs exhibited an enhanced fluorescence intensity (by about 3.5-fold), and their PLQY reached 6.2%. Due to the degradation of the copper shell and change in conformation of proteins, as well as the formation of $Zn(OH)_x$ at high pH values (>8), the optimum pH ranged from 6 to 8. CuS_x is an insoluble salt of copper and due to high oxidation/decomposition stability of Zn-modified Cu NCs in water, this sensor could be used for sensitive detection of sulfide ions by fluorescence quenching at 663 nm. The recovery of this ratiometric sensor in real water samples such as lake and tap water containing 20–80 μM S^{2-} was found to be 101–109.9%. This sensing system also showed a selective sensing performance for S^{2-} detection in water samples containing other common species.

Shen *et al.*[220] employed *in situ* synthesized Cu NCs for the detection of Cu^{2+} through an AIE phenomenon. Rapid reduction of Cu^{2+} ions in solution, and cluster formation using thiol-containing glutathione as both reducing and stabilizing agents occurred when THF, acetonitrile, and DMF were added. Aggregation of NCs induced a bright emission which increased through addition of more copper ions.

4.2.4. Detection of biomacromolecules and small biomolecules. Electrochemiluminescence (ECL) of metal NCs has been widely utilized in sensing and biosensing applications.[233] ECL efficacy of protein-templated metal NCs is restricted because of the IFE due to the tight arrangement of NCs that prevents the activation of internal emitters. Therefore, the realization of proper molecular arrangements through the controlled spatial distribution of NCs is of crucial importance, and DNA-templated NCs often show advantages over protein-templated NCs.[50,234] DNA structures have been employed for ECL detection of miRNA155.[50] Zhou *et al.*[50] prepared a DNA nanocrane structure with a manipulator on a glassy carbon electrode (GCE) through DNA hybridization and binding. Due to the tetrahedral structure of the nanocrane and the sequence of the manipulator, lateral and longitudinal separation of Cu NCs became possible. A strand displacement reaction, Mn^{2+} DNAzyme-assisted target recycling, and autonomous DNA walking created AT-rich dsDNA sequences on this structure (Fig. 5A). This strategy gave rise to ECL detection of miRNA155 on GCE in the presence of $S_2O_8{}^{2-}$ with a LOD of 36 attomolar (aM). In another study,[49] abasic sites of a dsDNA sequence were detected by DNA-templated Cu NCs. The NCs were formed from Cu^{2+} cations in the presence of AA and interacted with dsDNA. The chemically or enzymatically created DNA abasic sites impeded Cu NC formation, leading to an increase in the amount of unreacted Cu^{2+} cations, which in turn quenched the fluorescence intensity of carbon dots. This method could detect one or two abasic sites in a 35 bps DNA oligonucleotide. Borghei *et al.*[47] employed the DNA templating technique to detect miRNA155 having two different sequences; the first one had a 15-thymine-base and loop forming sequence, and the second had a poly thymine tail at one end. By measuring changes in the fluorescence intensity of Cu NCs, they detected miRNA with a lowest LOD of 2.2 pM in the linear range of 50 pM to 10 nM.[48]

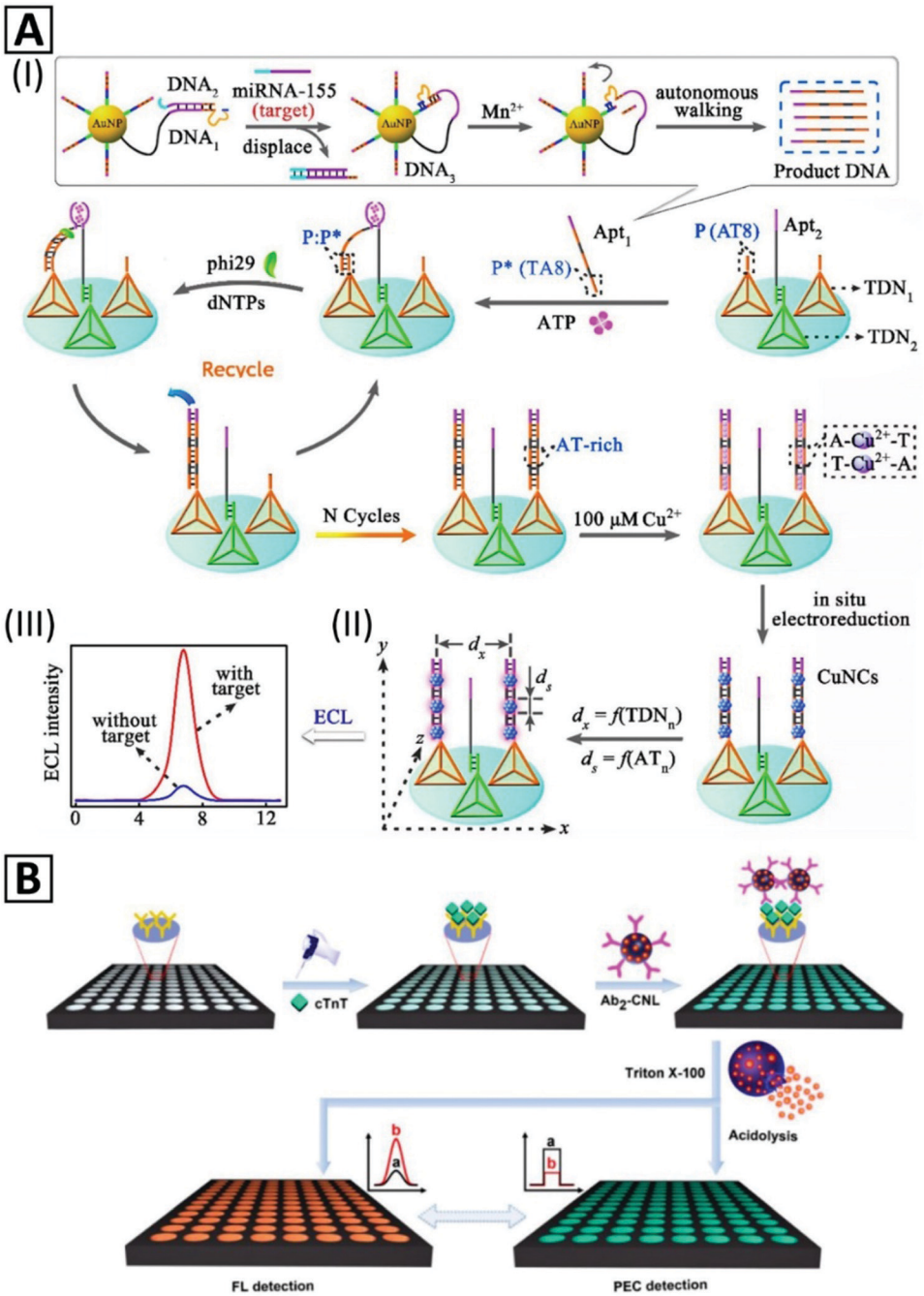

Fig. 5 (A) Schematic representation of miRNA155 detection based on nanocrane-like DNA structures. (I) Strand displacement by the target molecule leads to amplified production of DNA oligonucleotide containing an ATP binding sequence (Apt1). (II) Tetrahedral DNA nanostructures (TDN) modulate the efficiency of the ECL signal of Cu NCs which are formed by *in situ* electroreduction *via* programming the lateral spacing (dx) and size controlling (ds) through an AT periodic sequence. (III) ECL signal in the presence and absence of the target. Adapted with permission from ref. 50, Copyright 2018, ACS. (B) Representation of two complementary detection strategies (photoelectrochemical and fluorescent) for an immunoassay with Cu NC-encapsulated liposomes as signal generators. Adapted with permission from ref. 37, Copyright 2018, ACS.

Cu NCs were also used for protein detection. An immunoprobe was prepared by blocking unreacted sites of antibody-immobilized Pt NPs by BSA–Cu NCs.[235] The immunosensor could detect prostate specific antigen through a sandwich assay with a LOD of 145.69 fg mL^{-1} with a linear range from 0.5 pg mL^{-1} to 100 ng mL^{-1}. In another study,[37] an immunosensor was developed for detection of cardiac Troponin T (cTnT) antigen based on photoelectrochemical (PEC) signals generated after lysis treatment of secondary antibody-bonded liposomes. As illustrated in Fig. 5B, the secondary antibody was bonded to the external surface of Cu NC-encapsulated liposomes. This immunosensor could sensitively detect cTnT by a signal-off method through the PEC mechanism, with a LOD of 0.03 pg mL^{-1}.

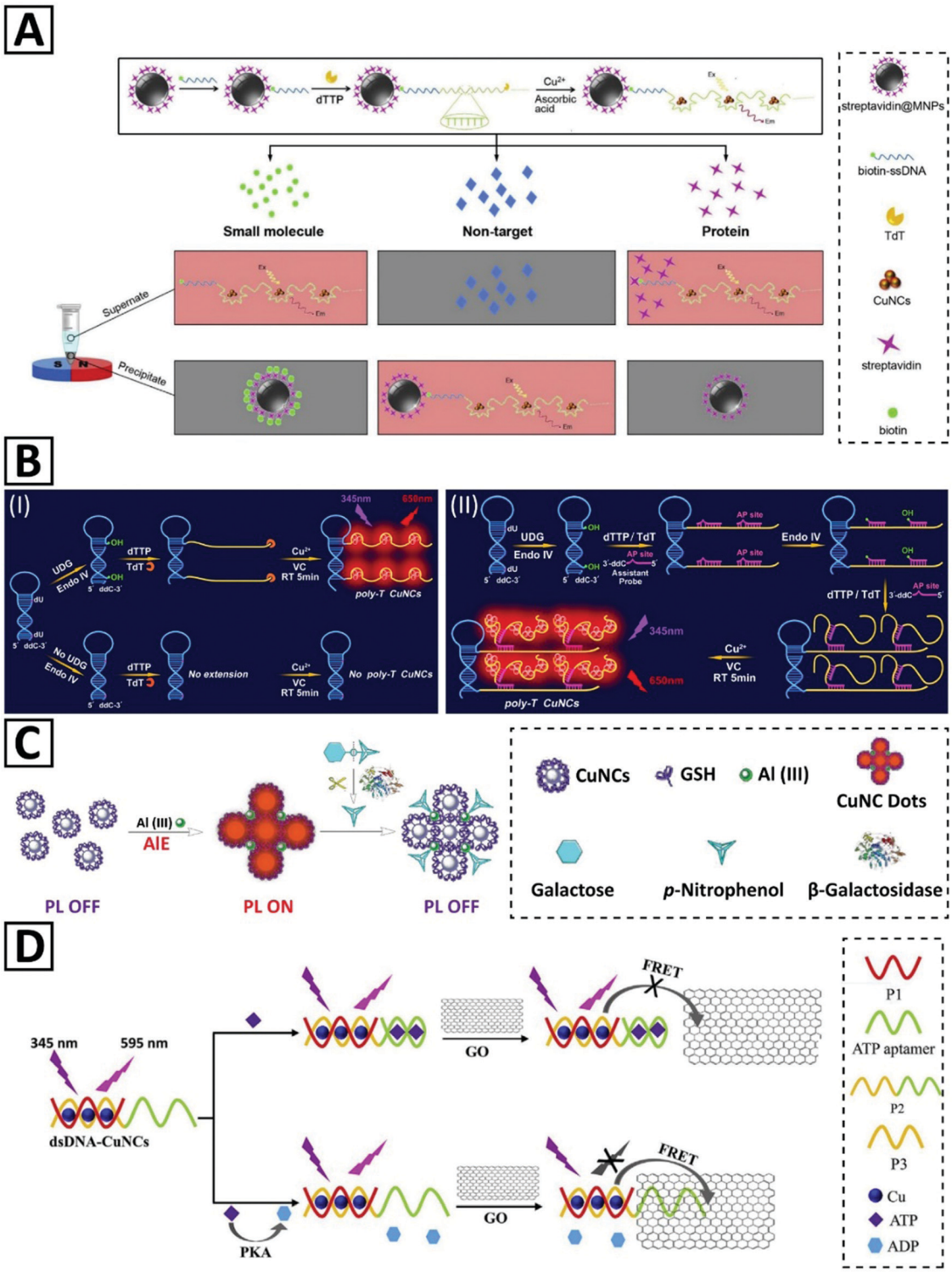

Fig. 6 (A) Representation of the detection strategy for small molecules and proteins relying on magnetic separation and opposite fluorescent signaling in the presence of Cu NCs. Adapted with permission from ref. 45, Copyright 2017, Elsevier. (B) Schematic illustration of (I) the proposed UDG assay principles and the roles of TdT and endonuclease IV in Cu NC template formation. (II) Hyperbranched extension of the Cu NC template helped by the assistant probe. Adapted with permission from ref. 46, Copyright 2019, Elsevier. (C) Schematic illustration of β-galactosidase activity measurement *via* emission quenching of aluminum-assisted self-assembled Cu NCs. Adapted with permission from ref. 105, Copyright 2017, RSC. (D) Schematic illustration of the PKA activity detection *via* a FRET-based fluorescent biosensor. Adapted with permission from ref. 40, Copyright 2018, Elsevier.

Cao *et al.*[45] presented a strategy for detecting a small molecule and its interacting protein, using streptavidin and biotin as a model (Fig. 6A). Protein molecules immobilized on magnetic nanoparticles (MNPs) were one part, and ssDNA oligonucleotides

with a small molecule at their 5′-end were another part of the detection system. The signal was generated *via* the formation of Cu NCs which were synthesized by a polythymin templating method. Supernatant or precipitant location of the generated signals determined the interacting proteins. This biosensor enabled detection of streptavidin and biotin in the linear range of 1–200 nM and 10–1000 nM, with LOD of 0.47 nM and 3.1 nM, respectively.

Hybrid nanostructures of Cu NCs and glucose oxidase (GOx) enzyme were employed for glucose sensing.[121] Enzymatic oxidation of glucose led to H_2O_2 production that would quench the emission of Cu NCs. The GO_x/Cu NC assembly selectively measured glucose with a LOD of 1.5 μM in a linear range of 5–100 μM. Another kind of biosensor for glucose *via* the turn-off fluorescence strategy has been designed based on lysozyme-stabilized Cu NCs (Lys-CCs).[236] A glucose biosensor using a pH-responsive fluorescent solution, a mixture of luminescent Cu NCs and $CaCO_3$ nanoparticles, and alginate, has been reported.[70] In the presence of glucose, the produced H^+ could release Ca^{2+} from $CaCO_3$ nanoparticles, which turned the solution into a gelated phase with an enhanced emission. This AIE-based sensor could detect glucose with a linear range of 0.1 to 2.0 mM and LOD of 3.2×10^{-5} M. Zhang *et al.*[237] employed OVA@Cu NCs for L-lysine (L-Lys) detection with a LOD of 5.5 μM and a linear range of 10 μM–1 mM. They showed that OVA@Cu NCs could selectively detect L-Lys among many other amino acids and cations based on the PL enhancement *via* coordination of copper by L-Lys functional groups and surface electron density increment on Cu NCs. Yang and co-workers[25] employed OVA@Cu NCs to detect Vitamin B1 (VB1) and doxycycline based on turn-off and turn-on PL strategies. VB1 quenched PL of OVA@Cu NCs through aggregation, while doxycycline enhanced the emission due to its strong interaction with OVA, and making a more compact structure. OVA–Cu NCs with a red emission at 625 nm and a PLQY of 3.95% were used for folic acid detection with a LOD of 0.18 μM. Evaluation of FA absorption (360 nm) and OVA–Cu NC excitation spectra (348 nm) as well as fluorescence lifetimes of Cu NCs in the presence and absence of FA indicated that the detection mechanisms should be the static quenching and the IFE.[36] Quenching of BSA–Cu NCs by rutin (a kind of flavonoid) through hydrogen bonding and electrostatic interactions between BSA and rutin was used for naked eye fluorescent detection in aqueous solution as well as on a paper filter.[34] *Via* the same mechanism, detection of mangiferin, a kind of flavonoid, was performed in real samples by BSA–Cu NCs.[238] In another biosensing method, Kojic acid, a fungal metabolite, was measured through Cu NCs FL quenching.[239] The fluorescence of BSA–Cu NCs was diminished due to its binding to copper ions and the formation of copper Kojate on the surface of Cu NCs.

Quenched fluorescence of NCs triggered by electron transfer of metal ions can be recovered by strong interactions between analytes and those ions.[240] The turn-on fluorescence of PEI–Cu NCs was employed for detecting biothiols (*e.g.* cysteine and GSH).[23] Herein, –SH functional groups interacted strongly with Cu^{2+} (introduced into the reaction mixture) as a quencher. Acetylcholinesterase (AChE), which is capable of hydrolyzing acetylthiocholine into thiocholine, has a strong tendency in forming a complex with Cu^{2+}; hence, it could be assayed by PEI–Cu NCs with a linear range of 3–200 mU mL^{-1} and LOD of 1.38 mU mL^{-1}.[23] This approach was also used for detecting an AChE typical inhibitor, tacrine.[23] In another study, a dual-emitting nanohybrid was prepared based on blue emitting carbon dots modified with 3-aminophenyl boronic acid (APBA-CDs) and BSA–Cu NCs for the detection of dopamine.[33] Red-emitting BSA–Cu NCs acted as an internal reference for measuring the PL quenching of APBA-CDs in the presence of dopamine, and a decrease in fluorescence intensity of APBA-CDs could be detected by the naked eye. Wang *et al.*[39] presented a molecular biology technique termed target-cycling strand displacement amplification (TCSDA) to detect adenosine 5′-triphosphate (ATP) in a broad dynamic range from 0.01 nM to 100 nM with a LOD of 5 pM. In the presence of ATP, an oligonucleotide hairpin probe containing an ATP aptamer sequence was structurally switched so that the TCSDA reaction was started by a DNA polymerase Klenow fragment (KF polymerase). This approach could detect ATP in a broad dynamic range from 0.01 nM to 100 nM, with a LOD of 5 pM. The PL intensity of PVP-stabilized Cu NCs was quenched after formation of a MnO_2–Cu NC complex through electrostatic interactions with MnO_2 nanospheres. GSH was selectively detected by this complex due to its capability of recovering the PL signal of Cu NCs (acting as donors) *via* digesting the MnO_2 nanospheres (energy acceptors). This FRET-based biosensor could detect GSH with a LOD of 17 μM.[21]

In addition to PL properties, the catalytic activity of Cu NCs was employed for biosensing, as well. Xu and co-workers[241] used the advantage of the peroxidase-mimetic activity of Cu NCs to detect cholesterol with a broad linear range of 0.05–10 mM and LOD of 1.5 μM. The assay was based on chemiluminescent signals produced by coupling two reactions. The first reaction was the oxidation process of cholesterol catalyzed by cholesterol oxidase enzyme, which produced H_2O_2 as a by-product. The second reaction was the luminol oxidation by H_2O_2, catalyzed by Cu NCs.

4.2.5 Enzyme activity detection. Monitoring the activity of enzymes catalyzing biological reactions in living cells is an important task, and metal NCs, including Cu NCs, have been widely employed for enzyme activity biosensing.[24,40,242–246] Two common strategies were utilized, including *in situ* synthesis of Cu NCs leading to the appearance of a fluorescence signal, especially for nucleic acid related enzymes, and the aggregation-induced emission (AIE).[247] Qing *et al.*[248] used micrococcal nuclease (MNase), a nucleic acid degrading enzyme, for detecting Staphylococcus aureus. They showed that in the absence of MNase, dsDNA with the aid of sodium ascorbate served as a template for the formation of Cu NCs with excitation/emission peaks located at 340/570 nm. The fluorescence turn-on strategy based on DNA-templated synthesis of Cu NCs was also used for the activity detection of enzymes like T4 polynucleotide kinase phosphatase,[43] DNA polymerase[231] and uracil-DNA glycosylase (UDG).[46] Both dsDNA and ssDNA can act as a template for the synthesis of Cu NCs. The UDG activity was detected through the

production of Cu NCs in a poly(T) tail ssDNA produced by a template-free DNA extension of terminal deoxynucleotidyl transferase.[46] UDG can remove uracil from the uracil-containing stem-loop DNA substrate with 3′-end block by 2′,3′-dideoxycytosine (ddC), providing sensitive UDG detection with a LOD of 50 μU mL^{-1}. The sensing scheme could be further improved *via* a branched amplification with the addition of an abasic site-contained poly(A) oligonucleotide, which was cleaved by endonuclease and its 3′-OH end was extended by TdT (Fig. 6B). The UDG enzyme activity has also been detected using the fluorescence approach, based on the 4′,6-diamidino-2-phenylindole (DAPI, λ_{em} = 452 nm) and poly(T) ssDNA templated Cu NCs (λ_{em} = 602 nm).[41] In the presence of UDG, three uracil-containing dsDNA substrates denatured, and one of ssDNA was partially hybridized with a helper dsDNA, which triggered exonuclease III digestion. The LOD of this sensor was reported to be 50 μU mL^{-1}.

The AIE effect is yet another common strategy that has been used for the activity detection of pyrophosphatase (PPi) by GSH-capped Cu NCs.[249,250] In the presence of Al^{3+}, the aggregation of Cu NCs occurred, leading to the PL enhancement due to AIE, providing a sensitive probe with a LOD of 1.3 mU mL^{-1}. Zhao *et al.*[68] prepared stable Cu NCs with improved AIE properties by employing a hydrophobic capping agent (4-methylthiophenol) during synthesis. The as-synthesized Cu NCs exhibited a weak emission due to their hydrophobic protecting ligands, but through subsequent processing, they were self-assembled into highly red emissive particles. Addition of a hydrophobic electron acceptor molecule (4-nitrophenol) could quench the emission of these Cu NCs by about 80%. Through this quenching strategy and using 4-nitrophenyl-β-D-galactopyranoside (NPGal) as the synthetic substrate for β-galactosidase enzyme, the enzymatic activity of β-galactosidase in serum could be measured with a LOD of 0.9 U L^{-1} in the linear range of 2.5–212.0 U L^{-1}. Huang *et al.*[105] used a similar strategy to monitor the β-galactosidase activity. They employed aluminum cations to self-assemble GSH-capped Cu NCs into so-called Cu NC dots with strong PL intensity, which was quenched upon enzymatic release of 4-nitrophenol from 4-nitrophenyl-β-D-galactopyranoside (Fig. 6C). The same PL-off or PL-on switching mechanism was used for the real-time monitoring of acid phosphatase activity, in which after hydrolyzing the bond between 4-nitrophenol and the phosphate group in p-nitrophenyl phosphate disodium, the PL quenching occurred.[251] In another study,[67] the acid phosphatase (ACP) enzyme activity was measured by redox-responsive emission of Cu NC aggregates. It was shown that D-penicillamine-capped Cu NCs with pH and temperature responsiveness could aggregate to form particles with stronger red luminescence. The existence of oxidant species such as free ferric ions (Fe^{3+}) could quench the PL intensity of CNC aggregates by 80% due to oxidation of copper atoms, providing an assay with 0.8 U L^{-1} LOD and a broad linear scope of up to 100 U L^{-1}. This strategy also was applied for ACP activity measurement in diluted serum samples as complex medium.[67]

Wang *et al.*[24] have introduced a novel assay for protein kinase A (PKA) activity based on the overlap of the emission of PEI-capped Cu NCs (with an emission peak around 515 nm) and the UV-Vis absorption spectrum of Au NPs. The already mentioned inner-filter effect (IFE) could quench PL of PEI–Cu NCs up to 59%. Peptide-functionalized Au NPs after phosphorylation by PKA enzyme with the assistance of adenosine 5′-triphosphate (ATP) molecules tend to aggregate in the presence of multivalent Zr^{4+} cations. This fluorescent biosensor for PKA activity measurement with a linear range of 0.1–6.0 U mL^{-1} and LOD of 0.038 U mL^{-1} also was employed for measuring the cellular kinase activity in HepG-2 cell lysates. In another study,[40] a biosensor for the PKA activity was developed based on the quenching effect of graphene oxide (GO) plates on dsDNA–Cu NCs through fluorescence resonant energy transfer (FRET) (Fig. 6D). Two-domain oligonucleotides including an ATP aptamer sequence were hybridized with a shorter complementary sequence as a template for Cu NC formation. Binding ATP molecules to aptamer sequences and folding ssDNA inhibited proximity between GO and dsDNA–Cu NCs and kept Cu NCs fluorescent. ATP hydrolysis to ADP by the PKA enzyme made the ATP domain of the oligonucleotide to be single-stranded, which could adsorb on GO *via* electrostatic and π–π stacking leading to PL quenching of dsDNA–Cu NCs. The linear range and LOD of this assay were 0.1–5.0 U mL^{-1} and 0.039 U mL^{-1}, respectively. A poly(AT–TA) dsDNA with a restriction site for EcoRI endonuclease was also used for endonuclease activity detection.[245] In the presence of the enzyme, dsDNA was cut even in the presence of reducing agent AA to affect the fluorescence intensity. This assay could detect EcoRI endonuclease concentration from 0.002 U μL^{-1} to 0.1 U μL^{-1}, with a LOD of 0.00087 U μL^{-1}.

4.2.6. Temperature and pH sensing. In many chemical and biological processes, both temperature and pH are factors which can significantly affect the kinetics and the reaction pathways. In biological, biomedical and pharmaceutical research, monitoring the fluctuations in temperature and pH during cellular metabolism and cell organelle functions plays an important role. Therefore, plenty of studies focused on the identification of fluorescent nanomaterials with pH or temperature responsive behavior,[252,253] and some of them have employed Cu NCs. Zhang *et al.*[31] prepared a blue-emitting silk fibroin/Cu NC composite, using it as a nanometer-sized pH sensor with a linear pH range from 6.08 to 10.05. The direct relationship between pH and PL intensity in different buffers such as BR, PBS, Tris–HCl and HEPES was demonstrated. The sensor behaved reversibly at least for 5 cycles, independent of the ionic strength and presence of a large number of cations. Xiaoqing *et al.*[254] used BSA-capped Cu NCs to detect the intracellular pH of RBL-2H3 cells and natural water. Their nano-pH meter exhibited a reversible response to pH up to 6 cycles in the pH range of 3.01 to 11.13.

Nano-thermometers have plenty of applications, especially in monitoring the temperature within biological cells and microfluidic devices.[255,256] Shi *et al.*[20] synthesized stable, blue-emitting Cu NCs with a PLQY of 12% and have shown that their fluorescence signal linearly decreased by 73% with increasing temperature from 20 to 75 °C, without any shifts of the emission peak (425 nm). Only 5% deviation was recorded after 10 cycles of heating and cooling between 20 and 75 °C. Han *et al.*[66] used bimetallic GSH–Cu/Ag NCs for temperature sensing; by introducing Ag ions during the synthesis of Cu NCs, 9-fold enhancement of

fluorescence intensity was attained. These bimetallic NCs with a strong orange-yellow emission and ionic strength stability showed a linear and inverse relationship between fluorescence intensity and temperature changes within 4–55 °C. Reversibility of the thermal response was demonstrated after 7 heating–cooling cycles without a decrease in the luminescence intensity. Bimetallic NCs were employed for confocal fluorescent imaging of HeLa cells after 24 h of incubation at three different temperatures (293 K, 303 K, and 313 K). The mechanism underlying fluorescence intensity quenching was ascribed to the aggregation of NCs.[216] Wang *et al.*[98] prepared highly fluorescent GSH-protected Cu NCs with QY 5% and used them for temperature monitoring and confocal imaging of MC3T3-E1 human cancer cells in the range of 15–45 °C.

4.3. Bioimaging

4.3.1. *In vitro* imaging. Cu NCs have been recognized as potential fluorescent probes for bioimaging, because of the features such as reasonably high PLQY, ultra-small size, flexible surface chemistry, and biocompatibility. By using different types of ligands and scaffolds, different kinds of Cu NCs for bioimaging have been prepared. Blue emitting Cu NCs (at 450 nm) were synthesized in lysozyme bed with a PLQY of 18%, and were used for labeling of HeLa cells;[152] blood compatibility tests confirmed their applicability for bioimaging. Likewise, blue emitting peptide-templated Cu NCs (with artificial sequence CLEDNN) were applied to HeLa labeling, without inducing any considerable toxicity.[155] PEI protected Cu NCs were used for labeling of 293T cells, which remained more than 75% viable after 24 h at 100 μg mL^{-1} concentration. PEI-capped Cu NCs were also employed for plasmid DNA condensation, which could be used as a DNA probe and non-viral vector for gene delivery.[22] Confocal microscopic studies demonstrated that blue emitting GSH–Cu NCs could localize in the membrane of three types of cancerous cells (MDA-MB-231, A549, and HeLa cells).[107] Tannic acid-stabilized Cu NCs were sensitive to ferric ions and could detect ferric ions inside A549 cells and serum samples.[4] BSA–Cu NCs were utilized as a pH probe in living cells by epifluorescence microscopy.[254] Cu NCs templated with dopamine were used for fluorescence painting and coding.[257]

Since UV irradiation necessary to excite blue emitting Cu NCs may damage the cells upon imaging, and induce the autofluorescence of the tissue, red emitting Cu NCs emerged as alternative probes. Wang and co-workers[13] used BSA–Cu NCs for low energy excitation at 524 nm and imaged 24 h-incubated CAL-27 cells at the peak emission of 625 nm. Kailasa's group[72] synthesized egg white supported Cu NCs with two emission wavelengths; confocal laser microscopy revealed a blue signal when excited by a 405 nm laser, and a green signal when excited by a 488 nm laser in *Bacillus subtilis*. When HeLa cells were treated with PEG-capped Cu NCs, confocal microscopy showed the ability of these Cu NCs to stain the nuclei through cellular uptake by membrane crossing without endocytosis.[5] In another study, transferrin (Tf) receptors were targeted by red emitting Trf–Cu NCs.[258] High expression of the Tf receptor on HeLa cells caused higher uptake of Tf–Cu NCs in comparison to 3T3 cells.

Temperature changes could be related to some unfavorable biological pathways of alive cells,[259,260] making temperature measurements combined with the cellular imaging quite important. Intracellular synthesis of Cu NCs has been performed for determination of temperature in living cells; Cu NCs with sizes of 2.4 ± 0.4 nm and red emission at 610 nm could be synthesized in malignant cell lines such as MDA-MB-231 *via* a specific biomolecular process.[73] Notably, this cannot be done in healthy cells, *e.g.* L02. Accumulation of these NCs in the target cells was efficient, and sensitivity of the fluorescence signal to the physiological temperature was high; the calibration curve for MDA-MB-231 cells showed 3.18% decrease in PL intensity per 1 °C temperature elevation. Owing to the critical role of Ca^{2+} in neurodegeneration and the importance of monitoring of Ca^{2+} pathways in neurons, Tian's group[261] developed a Ca^{2+}sensitive probe *via* Ca^{2+} ligand modified PEI templated Cu NCs (Fig. 7A-I). Alexa 660 NHS ester was conjugated to Cu NCs as a reference (Fig. 7A-II). The intensity of Cu NC PL in neurons was amplified based on the increase of Ca^{2+} concentration. The signal ratio of Cu NCs to reference sample could also be calibrated to a high concentration range sensor based on intracellular bioimaging. In another study, non-luminescent cysteine and chitosan protected Cu NCs were employed to specify cell differentiating at pH = 7.4. The kinetics of Cu NC aggregation inside different cell lines was dependent on the cell type so that a novel approach for detection of various cell lines could be developed only by green channel monitoring of confocal microscopy (Fig. 7B).[75,262]

4.3.2. *In vivo* imaging. Lung cancer, a five-year low survival rate disease (<15%), places serious threats on the global health,[263] and its early diagnosis helps to save time for the therapy of suffering patients. In recent years, researchers have paid special attention to positron emission tomography (PET) imaging, due to its unrestricted tissue penetration, higher sensitivity, and temporal resolution.[264] The progress of PET imaging agents able to target particular molecules is necessary for the advancement of clinically related PET techniques. ^{64}Cu as a PET imaging probe has been present in macrocyclic chelators. To put aside utilization of chelators, radioactive BSA-capped Cu NCs were synthesized for *in vivo* PET imaging. LHRH as a tumor target peptide was conjugated to BSA to form Cu NCs@BSA-LHRH,[76] which exhibited high radiolabeling constancy, rapid diffusion into the tumor, and high renal clearance. ^{64}Cu radioactivity measurements demonstrated that tumor uptake of Cu NCs@BSA-LHRH was 4 times greater than that of control Cu NCs@BSA. PET imaging by Cu NCs@BSA-LHRH as a contrast agent indicated sensitive and early precise diagnosis in a primary (orthotopic) lung cancer model (Fig. 7C).

4.4. Theranostic applications

Theranostic agents can be used in therapeutics and diagnostics at the same time.[8] Ghosh *et al.*[143] developed a hydrogel-based anticancer carrier containing Cu NCs and Cisplatin, using red fluorescent Cu NCs synthesized in an aqueous environment by using poly(vinylpyrrolidone) (PVP) stabilizer and dihydrolipoic acid. Composite fluorescent particles were sensitive to pH variations and exhibited emission changes from red to orange

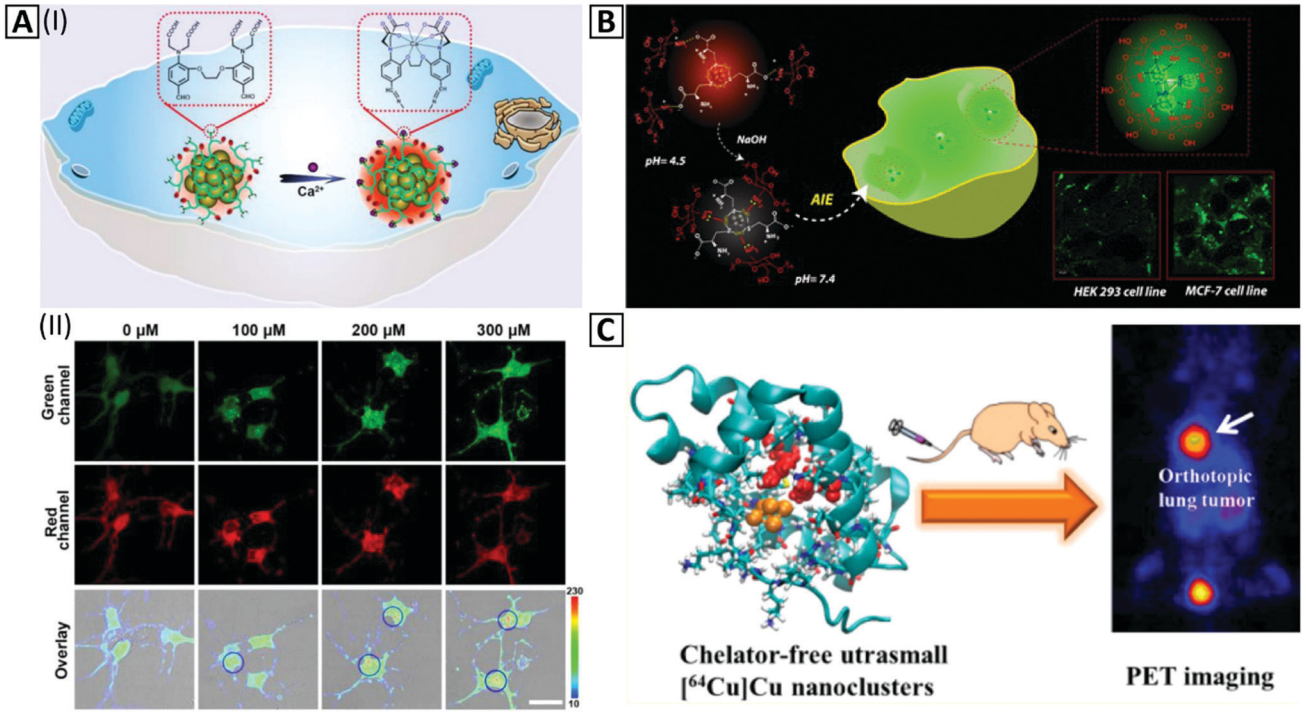

Fig. 7 (A-I) Schematic illustration of *in vitro* imaging based on the amplification of the PL intensity of the Cu NC@Alexa660 probe in the presence of Ca^{2+}. (A-II). Fluorescence confocal imaging exhibits amplification of the green channel intensity ratio to the constant signal intensity of the red channel inside neurons *via* an increase of Ca^{2+} concentration from 0–300 μM in the presence of 90 μg mL^{-1} of the Cu NC@Alexa660 probe. Adapted with permission from ref. 261, Copyright 2019, ACS. (B) Schematic illustration of *in vitro* imaging of HEK 293 and MCF-7 cells by red-emitting Cu NCs at pH = 4.5, which change their color to green at pH = 7.4 *via* the AIE effect inside the cell cytoplasm. Adapted with permission from ref. 75, Copyright 2018, ACS. (C) *In vivo* PET imaging and organ distribution study after 2 h intravenous injection of Cu NCs @BSA-LHRH. Adapted with permission from ref. 76, Copyright 2015, ACS.

through adjustment of the pH in the range of 4 to 8.5. Fluorescence microscopy showed how this kind of nanocarrier can be used for mammalian cell uptake monitoring; synergetic anticancer activity was attained by coupling the therapeutic effect of Cisplatin alongside with the ability of Cu NCs in killing cancerous cells through generation of reactive oxygen species (ROS). Goswami *et al.*[77] prepared blue emitting Tf-templated Cu NCs and combined them with Dox through electrostatic interactions to formulate sphere-shaped Tf–Cu NC–Dox NPs for active theranostics. Due to FRET occurring in this system, Tf–Cu NC–Dox NPs displayed significant red emission, while the release of Dox inside the cytoplasm of Tf receptor over-expressed cancer cells restored the blue emission of Cu NCs. A synergistic effect of the ROS generation by Tf–Cu NCs and the anticancer activity of Dox for the therapy of mouse models has been demonstrated. Another study revealed that temozolomide loaded positron emitting Cu NCs could upgrade a PET contrast agent to a theranostics agent for glioblastoma.[78]

4.5. Other bioapplications

In addition to applications of Cu NCs considered above, there are a few other emerging areas where they can be of interest. For instance, biological staining is frequently used to mark cells in flow cytometry, and to flag proteins or nucleic acids in gel electrophoresis.[265] Zhu *et al.*[266] developed a method for *in situ* staining of DNA in a polyacrylamide gel through the formation of Cu NCs in the presence of a DNA template. Cu NCs have also been utilized for the detection of single nucleotide polymorphisms, which are responsible for various genetic problems of human health.[267] Since dsDNA affects the Cu NC environment and thus changes the fluorescence intensity, a "mix-and-measure" strategy has been employed for mismatch detection of dsDNA. Cu NCs can also serve as smart probes opening opportunities for fast and economical bioanalysis.[268]

In recent years, nano-bioelectronics has attracted significant attention as a rapidly expanding interdisciplinary field which utilizes nanomaterials to overcome some current limitations in bioelectronics.[269] DNA nanowires are promising materials for this purpose, while Cu NCs with resistance to charge transfer can be employed as the key element for the "ON–OFF" process. To exhibit practical aspects of this phenomena, one end of dsDNA was immobilized on the surface of gold electrodes, and another end was tagged by methylene blue (a redox-active agent). In the presence of AA, Cu^{2+} was reduced to Cu^{0} and deposited on the DNA scaffold, which resulted in a switch-off of the charge transfer path. The process was reversible and repetitive by utilizing oxidants that caused the stripping of Cu NCs.[270]

The antimicrobial effect of Cu NCs has recently been explored.[110] Baghdasaryan *et al.* showed the dose-dependent bactericidal capability of GSH-capped Cu NCs: at low cluster

concentrations the growth of bacteria was slowed down, and at high dosages (≥ 250 μg mL^{-1}) the bacterial replication was fully restricted. Antimicrobial action of metal NCs has been ascribed to intracellular ROS generation.[271] To utilize the high antibacterial performance of metal NCs, Ag, Cu, and Au NCs@Bacitracin were synthesized by Wang and coworkers.[272] Bacitracin as a peptide antibiotic can damage the bacterial membrane; hence, the synergy of the membrane damage and the ROS generation by different MNCs@Bacitracin clusters could be attained. It was demonstrated that Ag NCs@Bacitracin was the most powerful antibacterial agent against *S. aureus*. Comparative results of zone inhibitions, growth curve, percentage of PI stained bacteria, and relative ROS levels are provided in Fig. 8. Cu NC-doped kanamycin-loaded hydroxyapatite NPs were introduced as an antibiofilm and antibacterial agent.[273]

4.6. Applications in photovoltaics and optoelectronics

4.6.1. Light harvesting. Photosynthesis is a classical example of light-harvesting systems based on natural composite materials, on which base a number of photovoltaic and optoelectronic applications have been developed.[274] Different from numerous studies on Au NCs,[275,276] utilizing Cu NCs in light harvesting and charge transfer nanocomposites has been rather rare, so far. Patra's group[79] produced a light harvesting nanocomposite by electrostatic interactions between the carboxylate groups of cysteine-capped Cu NCs and imidazole moieties of functionalized reduced graphene oxide (ImRGO) (Fig. 9A). The absorption spectrum of the nanocomposite was the sum of the Cu NCs and ImRGO spectra, while PL studies revealed that 87% quenching of the emission intensity of Cu NCs occurred, accompanied by a significant decrease of the average PL decay time of the Cu NCs in the composite. The positions of HOMO/LUMO levels signified electron transfer from Cu NCs to ImRGO, due to the lower lying work function of the latter (Fig. 9B).

4.6.2. Solar cells. γ-Phase copper iodide (γ-CuI) is a well-known p-type semiconductor, but its fabrication using wet chemical methods is challenging. Zheng's group[80] used Cu_{53} NCs soluble in ether to deposit them on organolead halide perovskite films, with subsequent iodination to form high-quality γ-CuI films (Fig. 9C). The energy level diagram of the resulting solar cell device signified the injection of holes from the perovskite to the γ-CuI film (Fig. 9D), which attained 14.3% efficiency with a minimal hysteresis.[80]

4.6.3. Light-emitting devices. Light emitting Cu NCs have been often employed as phosphors in down conversion LED prototypes. Wang *et al.*[144] synthesized high PLQY Cu NCs with combined red and green emissions and constructed down-conversion white light-emitting devices (WLEDs) with a high color rendering index of 92. First, blue emitting PVP-protected Cu NCs with a PLQY of 8% were synthesized in an aqueous phase and treated with GSH to enhance their PLQY to 27% with a red shift in the emission peak. This enhancement was attained *via* the metal-chelating capability of thiol motifs of GSH, combined with electron-rich carboxyl and amino functional groups of PVP.

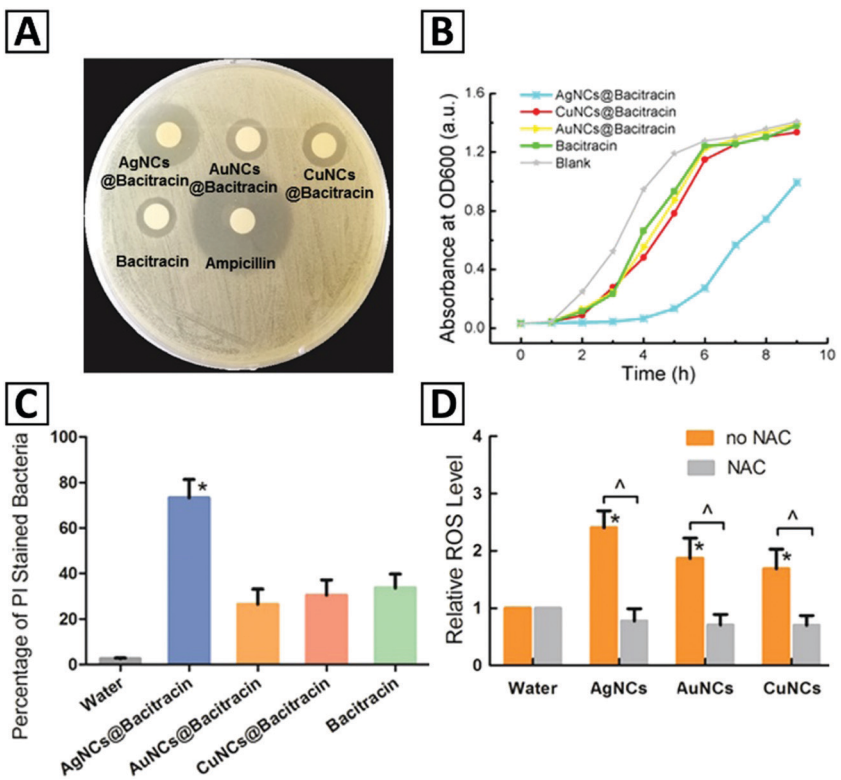

Fig. 8 (A) Zone inhibitions against *S. aureus* by Ag, Au, Cu NCs@Bacitracin, bacitracin, and ampicillin. (B) *S. aureus* growth curve in the presence of Ag, Au, and Cu NCs@ Bacitracin. (C) The percentage of stained bacteria cells with PI in the presence of water, Ag, Au, Cu NCs@ Bacitracin, and bacitracin. (D) ROS levels in bacteria cells treated with Ag, Au, and Cu NCs@Bacitracin; ROS levels are for two separate groups treated by water with/out NAC. Adapted with permission from ref. 272, Copyright 2019, ACS.

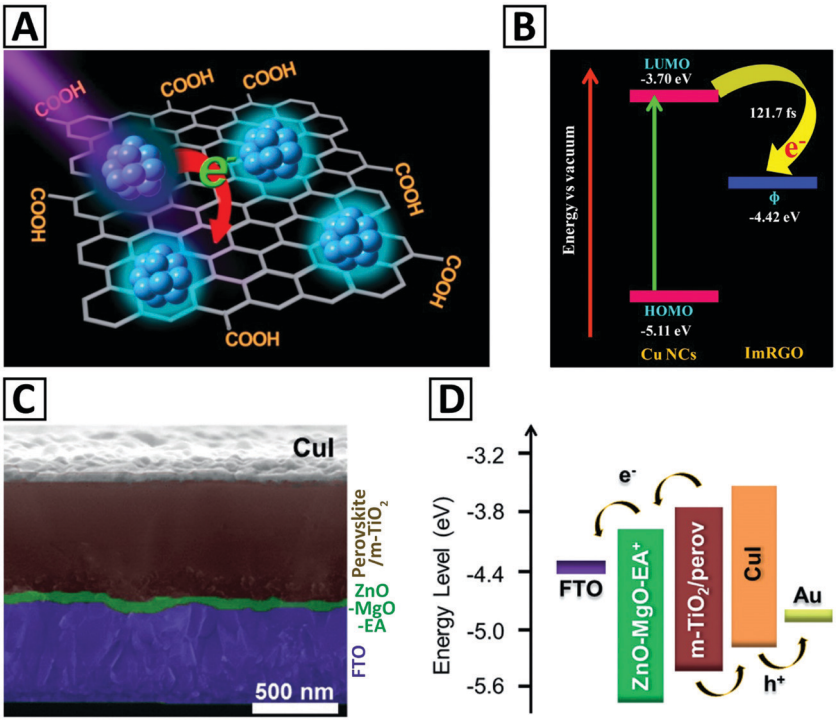

Fig. 9 (A) Schematic illustration of a Cu NCs/ImRGO nanocomposite, and (B) positions of the HOMO–LUMO levels of Cu NCs and work function (ϕ) of ImRGO. Adapted with permission from ref. 79, Copyright 2018, ACS. (C) Cross-sectional scanning electron microscopy image of a CuI film made from Cu_{53} NCs deposited on a lead halide perovskite film through iodization, and (D) energy level diagram of the CuI-based perovskite solar cell. Adapted with permission from ref. 80, Copyright 2019, Wiley-VCH.

Wu *et al.*[81] utilized luminescence enhancement of 1-dodecanethiol (DT)-stabilized Cu NCs to fabricate WLEDs. They showed that self-assembly of Cu NCs to ribbons and sheets resulted in favorable emission changes, amplifying cuprophilic interactions and preventing intramolecular rotation and vibration of the DT stabilizer. This intensified the emission intensity with a blue shift, displaying different thermochromic and mechanochromic luminescence attributes. It was also suggested that surface defects moderately enhanced the ratio of Cu^{+}-to-Cu^{0}, which boosted radiative states of excited electrons *via* the effect on the ligand-to-metal–metal charge transfer (LMMCT).[102] Blue-green, yellow, and red emitting Cu NCs were prepared and utilized as phosphors to construct WLEDs. By employing thiophenols with different substitutes as a ligand, the emission color and intensity of self-assembled Cu NC nanoribbons could also be tuned;[82] using this strategy, various types of nanoribbons with high PLQY could be prepared and employed for the fabrication of WLEDs.

Another strategy for tuning fluorescence color is metal doping.[277] Liu *et al.*[202] showed that Au^{+} doping upon preparation of Cu nanosheets increased their PL intensity with an emission red-shift. The Au doping induced metallophilic interactions of Au^{+}–Cu^{+}, facilitating excited electrons to experience the radiative relaxation, owing to changes in the ligand-to-metal charge transfer (LMCT) and/or LMMCT. The Au doping also decreased the original Cu-centered triplet energy state inducing an emission red-shift. They revealed that introducing 0.3% Au was enough to give rise to 4-fold PL enhancement with a 100 nm emission red-shift. Such Au^{+}-doped Cu nanosheets have been applied as phosphors for WLED fabrication.

The AIE effects of luminescent metal NCs have also been utilized for fabrication of WLEDs.[101,122,278] As already mentioned above, AIE is able to significantly enhance the emission of the Cu NCs by suppression of the rotation and vibration of their capping ligands.[279] Wang *et al.*[18] used a solvent-induced aggregation method for synthesis of orange emitting aggregated GSH-capped Cu NCs, which showed PLQY of 24% and 43% in solution and solid state, respectively. In parallel, blue emitting Cu NCs@ PVP were synthesized, with a PLQY of 14%. Both monochrome blue or orange LEDs, and WLEDs were fabricated by depositing respective powders on commercial GaN LED chips providing 370 nm excitation (Fig. 10).[101] WLEDs combining blue emitting sulfur QDs with the aggregated orange emitting Cu NCs have been demonstrated, as well.[280] The same group used *in situ* aggregation of Cu NCs in a carboxylated polyurethane matrix to produce remote dual blue/orange emitting composite films,[278] which were thermally and mechanically stable, and stretchable. The PLQY of the films was as high as 18% and the CIE chromaticity coordinate was (0.34, 0.29). A dehydration-triggered aggregation of GSH capped Cu NCs occurring in a PVP/poly(vinyl alcohol) matrix resulted in the formation of flexible, large-area polymer composite films with a high PLQY of 30%, which have been used for fabrication of bright orange LEDs.[281] A similar dehydration mechanism was used to fabricate protective transparent UV shielding films,[282] and biocompatible hypromellose–chitosan copolymers with AIE improved the emission of the Cu NCs reaching 42%.[83]

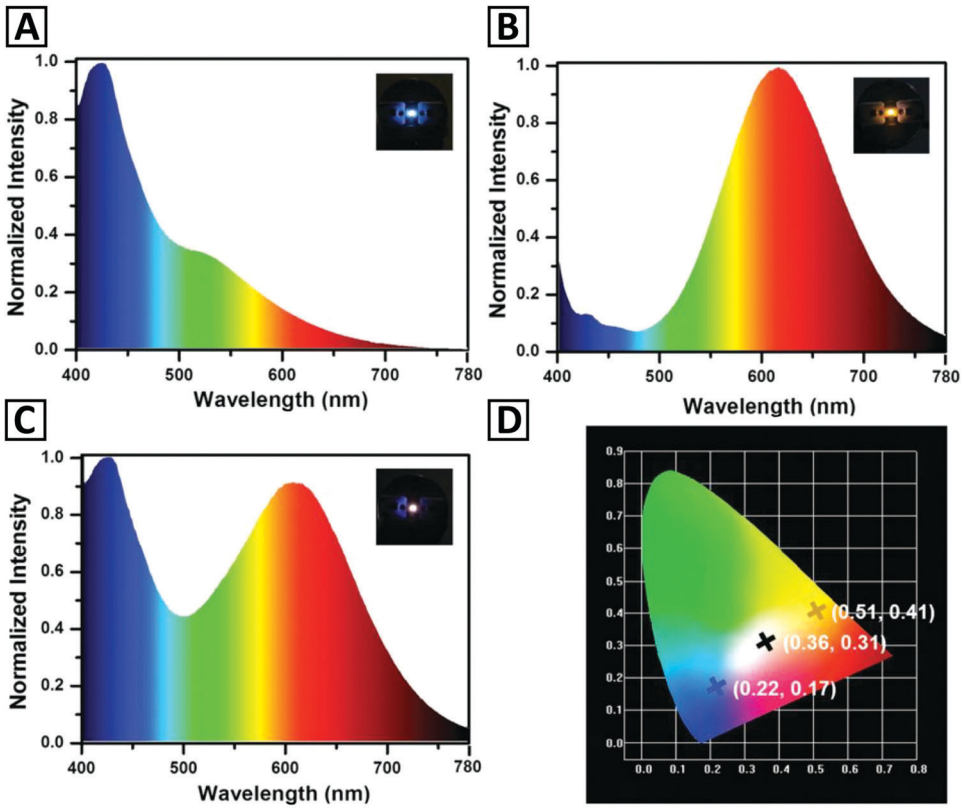

Fig. 10 Emission spectra of monochrome down-conversion LEDs fabricated by using (A) blue emitting Cu NCs and (B) orange emitting Cu NCs. Panel (C) shows an emission spectrum of the WLED fabricated by a combination of these two kinds of Cu NCs. Insets in (A–C) provide photographs of operating blue, orange and white LEDs; while panel (D) shows CIE coordinates of three respective LEDs. Reproduced with permission from ref. 101, Copyright 2016, Wiley-VCH.

5. Conclusions and outlook

In this review, rapidly expanding deployment of Cu NCs in a series of important applications such as catalysis, chemical and biological sensing, bioimaging, theranostics, and fabrication of LEDs is summarized. Extensive up to date research has been carried out on developing viable methods for the synthesis of these promising nanomaterials. One important factor that controls the properties of Cu NCs is related to the nature of their functional capping agents. Thus, the main thrust in the field of synthesis of Cu NCs is to identify the most appropriate capping agents (ligands) and related templates. Due to the favorable price considerations and availability of precursor materials, practical catalytic applications of Cu NCs are expected to become widespread as compared to noble metal catalysts, *i.e.* silver and gold. Also for this application, in order to obtain the desired catalytic activity in appealing reactions *e.g.* reduction, oxidation, and hydrogen generation, several capping agents/supporting ligands have been investigated. Development of theoretical methods which predict the catalytic performance of Cu NCs or alloys can facilitate the process of synthesis and introduction of catalysts implemented in some industrial applications in the future. Most of the sensors that have been designed using Cu NCs exploit their emission (both quenching and enhancement) as the main analytical signal. Capping ligands or stabilizing scaffolds play an important role in the detection mechanism. As in other fluorescent probes, the emission intensity can decrease, increase, or get quenched as a result of interactions with the analyte; thereby, plenty of detection strategies could be employed for different kinds of target molecules. Additionally, combining two or more signal amplification strategies such as molecular biology-based techniques with methods like *in situ* synthesis of Cu NCs can enhance the detection capability of the (bio)sensor and significantly lower the detection limits. Non (or low) toxicity, biocompatibility, and low price make Cu NCs attractive for designing label-free fluorescence sensors. Herein, a variety of analyte classes have successfully been analyzed. There are still drawbacks in this field which are currently inherent to Cu NCs, such as moderate PL QY and higher susceptibility to oxidation; improvement of these aspects has been in the focus of researcher's attention. Using various types of scaffolds, which can be conjugated to targeting agents, Cu NCs have also been utilized as fluorophores for both *in vitro* and *in vivo* bioimaging. Bioimaging can be used to characterize different types of cancer cells, nanothermometry, and estimation of concentration of analytes inside cells. Cu NCs are able to generate ROS inside eukaryotic and prokaryotic cells and to induce cell death as anticancer and antibacterial agents. ^{64}Cu as a PET imaging probe has been used for the design of new types of PET contrast agents. Recently, Cu NCs have been also used in photovoltaics, which may provide

new opportunities for fabrication of solar cells. Light-emitting Cu NCs were also employed as phosphors in down-conversion LEDs, both monochrome ones, in particular in WLEDs; however, both efficiency and long-term stability of such devices still require massive improvements before their actual practical use.

Conflicts of interest

There are no conflicts to declare.

Acknowledgements

We acknowledge financial support from the Iran National Science Foundation (INSF No. 95-S-48740), Sharif University of Technology (Grant No. QA970816), the Research Grant Council of Hong Kong S.A.R. (CityU11305617), and the Science Technology and Innovation Committee of Shenzhen Municipality (JCYJ20170818104224667).

References

1 J. Wilcoxon and B. L. Abrams, *Chem. Soc. Rev.*, 2006, **35**, 1162–1194.
2 X. Hu, T. Liu, Y. Zhuang, W. Wang, Y. Li, W. Fan and Y. Huang, *TrAC, Trends Anal. Chem.*, 2016, **77**, 66–75.
3 L. Zhang and E. Wang, *Nano Today*, 2014, **9**, 132–157.
4 H. Cao, Z. Chen, H. Zheng and Y. Huang, *Biosens. Bioelectron.*, 2014, **62**, 189–195.
5 M. J. Barthel, I. Angeloni, A. Petrelli, T. Avellini, A. Scarpellini, G. Bertoni, A. Armirotti, I. Moreels and T. Pellegrino, *ACS Nano*, 2015, **9**, 11886–11897.
6 X. Liu and D. Astruc, *Coord. Chem. Rev.*, 2018, **359**, 112–126.
7 Z. Wang, B. Chen and A. L. Rogach, *Nanoscale Horiz.*, 2017, **2**, 135–146.
8 S. Shahsavari and F. Behroozi, *J. Nanomed. Res.*, 2016, **3**, 00069.
9 X. Jia, X. Yang, J. Li, D. Li and E. Wang, *Chem. Commun.*, 2014, **50**, 237–239.
10 Z. Wu, Y. Li, J. Liu, Z. Lu, H. Zhang and B. Yang, *Angew. Chem., Int. Ed.*, 2014, **53**, 12196–12200.
11 L. D. Pachón, J. H. Van Maarseveen and G. Rothenberg, *Adv. Synth. Catal.*, 2005, **347**, 811–815.
12 A. W. Cook, Z. R. Jones, G. Wu, S. L. Scott and T. W. Hayton, *J. Am. Chem. Soc.*, 2017, **140**, 394–400.
13 C. Wang, C. Wang, L. Xu, H. Cheng, Q. Lin and C. Zhang, *Nanoscale*, 2014, **6**, 1775–1781.
14 Z. Jin, C. Liu, K. Qi and X. Cui, *Sci. Rep.*, 2017, **7**, 39695.
15 R. Cai, P. R. Ellis, J. Yin, J. Liu, C. M. Brown, R. Griffin, G. Chang, D. Yang, J. Ren and K. Cooke, *Small*, 2018, **14**, 1703734.
16 B. Eren, D. Zherebetskyy, L. L. Patera, C. H. Wu, H. Bluhm, C. Africh, L.-W. Wang, G. A. Somorjai and M. Salmeron, *Science*, 2016, **351**, 475–478.
17 B. Sarkar, P. Prajapati, R. Tiwari, R. Tiwari, S. Ghosh, S. S. Acharyya, C. Pendem, R. K. Singha, L. S. Konathala and J. Kumar, *Green Chem.*, 2012, **14**, 2600–2606.
18 R. Aparna, J. A. Devi, P. Sachidanandan and S. George, *Sens. Actuators, B*, 2018, **254**, 811–819.
19 Y. Li, L. Feng, W. Yan, I. Hussain, L. Su and B. Tan, *Nanoscale*, 2019, **11**, 1286–1294.
20 Y. E. Shi, S. Luo, X. Ji, F. Liu, X. Chen, Y. Huang, L. Dong and L. Wang, *Dalton Trans.*, 2017, **46**, 14251–14255.
21 T. Li, Z. Wang, D. Jiang, H. Wang, W. F. Lai, Y. Lv and Y. Zhai, *Sens. Actuators, B*, 2019, **290**, 535–543.
22 C. Wang, Y. Yao and Q. Song, *Colloids Surf., B*, 2016, **140**, 373–381.
23 J. Yang, N. Song, X. Lv and Q. Jia, *Sens. Actuators, B*, 2018, **259**, 226–232.
24 S. Song, C. Wang, Y. Zhao, T. Hu, X. Zhou, T. Zhao, M. Yang and Q. Lin, *Part. Part. Syst. Charact.*, 2018, **35**, 1700471.
25 K. Yang, Y. Wang, C. Lu and X. Yang, *J. Lumin.*, 2018, **196**, 181–186.
26 A. Yousefzadeh, J. Hassanzadeh, S. M. J. Mousavi and M. Yousefzadeh, *Sens. Actuators, B*, 2019, **154–162**, 154–162.
27 R. S. Aparna, J. S. Anjali Devi, R. R. Anjana, J. Nebu and S. George, *Sens. Actuators, B*, 2019, **291**, 298–305.
28 G. Zhang, R. Wang, L. Shi, C. Zhang, Y. Zhang, Y. Zhou, C. Dong, G. Li and S. Shuang, *Sens. Actuators, B*, 2019, **279**, 361–368.
29 S. Xu, K. Zhou, D. Fang and L. Ma, *Molecules*, 2019, **24**, 95.
30 Z. Shojaeifard, N. Heidari and B. Hemmateenejad, *Spectrochim. Acta, Part A*, 2019, **209**, 202–208.
31 G. Zhang, T. Xu, H. Du, Y. Qiao, X. Guo, L. Shi, Y. Zhang, S. Shuang, C. Dong and H. Ma, *J. Mater. Chem. C*, 2016, **4**, 3540–3545.
32 R. Rajamanikandan and M. Ilanchelian, *Mater. Sci. Eng., C*, 2019, **98**, 1064–1072.
33 W. He, R. Gui, H. Jin, B. Wang, X. Bu and Y. Fu, *Talanta*, 2018, **178**, 109–115.
34 Y. Wang, T. Chen, Q. Zhuang and Y. Ni, *Talanta*, 2018, **179**, 409–413.
35 R. Aparna, J. A. Devi, R. Anjana, J. Nebu and S. George, *Analyst*, 2019, **144**, 1799–1808.
36 X. Li, X. Wu, F. Zhang, B. Zhao and Y. Li, *Talanta*, 2019, **195**, 372–380.
37 L.-P. Mei, X.-Y. Jiang, X.-D. Yu, W.-W. Zhao, J.-J. Xu and H.-Y. Chen, *Anal. Chem.*, 2018, **90**, 2749–2755.
38 J. Li, W. Fu, J. Bao, Z. Wang and Z. Dai, *ACS Appl. Mater. Interfaces*, 2018, **10**, 6965–6971.
39 Y. M. Wang, J. W. Liu, L. Y. Duan, S. J. Liu and J. H. Jiang, *Microchim. Acta*, 2017, **184**, 4183–4188.
40 M. Wang, Z. Lin, Q. Liu, S. Jiang, H. Liu and X. Su, *Anal. Chim. Acta*, 2018, **1012**, 66–73.
41 Y. Ling, J. Zhou, X. F. Zhang, X. H. Wang, N. B. Li and H. Q. Luo, *Sens. Actuators, B*, 2019, **286**, 46–51.
42 R. Li, Q. Liu, Y. Jin and B. Li, *Sens. Actuators, B*, 2019, **281**, 28–33.
43 X. Zhang, Q. Liu, Y. Jin and B. Li, *Microchim. Acta*, 2019, **186**, 3.
44 F. M. Moghadam and M. Rahaie, *Biosens. Bioelectron.*, 2019, **132**, 186–195.
45 J. Cao, W. Wang, B. Bo, X. Mao, K. Wang and X. Zhu, *Biosens. Bioelectron.*, 2017, **90**, 534–541.

46 G. Liu, W. He and C. Liu, *Talanta*, 2019, **195**, 320–326.
47 Y.-S. Borghei, M. Hosseini and M. R. Ganjali, *Microchim. Acta*, 2017, **184**, 2671–2677.
48 Y.-S. Borghei, M. Hosseini, M. R. Ganjali and S. Hosseinkhani, *Sens. Actuators, B*, 2017, **248**, 133–139.
49 S. Singh, M. K. Singh and P. Das, *Sens. Actuators, B*, 2018, **255**, 763–774.
50 Y. Zhou, H. Wang, H. Zhang, Y. Q. Chai and R. Yuan, *Anal. Chem.*, 2018, **90**, 3543–3549.
51 Y. Nerthigan, A. K. Sharma, S. Pandey and H.-F. Wu, *Microchim. Acta*, 2019, **186**, 130.
52 A. Hatefi, E. Rahimpour, M. Khoubnasabjafari, M. Edalat, V. Jouyban-Gharamaleki, S. Alvani-Alamdari, A. Nokhodchi, M. H. Pournaghi-Azar and A. Jouyban, *Microchim. Acta*, 2019, **186**, 194.
53 H. Liu, X. Gao, X. Zhuang, C. Tian, Y. Li and A. Rogach, *Analyst*, 2019, **144**, 4425–4431.
54 Y. Ma, Y. Yu, B. Lin, L. Zhang, Y. Cao and M. Guo, *Microchim. Acta*, 2019, **186**, 206.
55 G. Hambarde, S. Bothra, Y. Upadhyay, R. K. Bera and S. K. Sahoo, *Microchem. J.*, 2019, **147**, 899–904.
56 S. Han and X. Chen, *Spectrochim. Acta, Part A*, 2019, **210**, 315–320.
57 Z. Shen, C. Zhang, X. Yu, J. Li, B. Liu and Z. Zhang, *Microchem. J.*, 2019, **145**, 517–522.
58 Y.-S. Lin, T.-C. Chiu and C.-C. Hu, *RSC Adv.*, 2019, **9**, 9228–9234.
59 Z. Wen, S. Song, C. Wang, F. Qu, T. Thomas, T. Hu, P. Wang and M. Yang, *Sens. Actuators, B*, 2019, **282**, 9–15.
60 Y. Cheng, F. Sun and Y. Zhou, *J. Lumin.*, 2018, **197**, 376–382.
61 C. Boonmee, V. Promarak, T. Tuntulani and W. Ngeontae, *Talanta*, 2018, **178**, 796–804.
62 J. R. Bhamore, B. Deshmukh, V. Haran, S. Jha, R. K. Singhal, N. Lenka, S. K. Kailasa and Z. V. P. Murthy, *New J. Chem.*, 2018, **42**, 1510–1520.
63 L. Kong, X. Chu, C. Wang, H. Zhou, Y. Wu and W. Liu, *Nanoscale*, 2018, **10**, 1631–1640.
64 T. Chen, Z. Zhang, Y. Wang and Y. Ni, *Gaodeng Xuexiao Huaxue Xuebao/Chemical Journal of Chinese Universities*, 2017, **38**, 1737–1741.
65 J. Cang, C. W. Wang, P. C. Chen, Y. J. Lin, Y. C. Li and H. T. Chang, *Anal. Methods*, 2017, **9**, 5254–5259.
66 B. Han, X. Hou, R. Xiang and G. He, *Anal. Methods*, 2017, **9**, 4028–4032.
67 M. Zhao, H. Feng, J. Han, H. Ao and Z. Qian, *Anal. Chim. Acta*, 2017, **984**, 202–210.
68 M. Zhao, Z. Qian, M. Zhong, Z. Chen, H. Ao and H. Feng, *ACS Appl. Mater. Interfaces*, 2017, **9**, 32887–32895.
69 Y. Hu, Y. He, Y. Han, Y. Ge, G. Song and J. Zhou, *Microchim. Acta*, 2019, **186**, 5.
70 S. Gou, Y.-e. Shi, P. Li, H. Wang, T. Li, X. Zhuang, W. Li and Z. Wang, *ACS Appl. Mater. Interfaces*, 2019, **11**, 6561–6567.
71 S. Yang, X. Sun and Y. Chen, *Mater. Lett.*, 2017, **194**, 5–8.
72 J. R. Bhamore, S. Jha, A. K. Mungara, R. K. Singhal, D. Sonkeshariya and S. K. Kailasa, *Biosens. Bioelectron.*, 2016, **80**, 243–248.
73 J. Ye, X. Dong, H. Jiang and X. Wang, *J. Mater. Chem. B*, 2017, **5**, 691–696.
74 J.-M. Xia, X. Wei, X.-W. Chen, Y. Shu and J.-H. Wang, *Microchim. Acta*, 2018, **185**, 205.
75 A. Dutta, U. Goswami and A. Chattopadhyay, *ACS Appl. Mater. Interfaces*, 2018, **10**, 19459–19472.
76 F. Gao, P. Cai, W. Yang, J. Xue, L. Gao, R. Liu, Y. Wang, Y. Zhao, X. He and L. Zhao, *ACS Nano*, 2015, **9**, 4976–4986.
77 U. Goswami, A. Dutta, A. Raza, R. Kandimalla, S. Kalita, S. S. Ghosh and A. Chattopadhyay, *ACS Appl. Mater. Interfaces*, 2018, **10**, 3282–3294.
78 A. Choksi, X. Zhang, G. S. Heo, H. Luehmann and Y. Liu, *J. Nucl. Med.*, 2018, **59**, 1122.
79 S. Maity, D. Bain, K. Bhattacharyya, S. Das, R. Bera, B. Jana, B. Paramanik, A. Datta and A. Patra, *J. Phys. Chem. C*, 2017, **122**, 13354–13362.
80 P. Yuan, R. Chen, X. Zhang, F. Chen, J. Yan, C. Sun, D. Ou, J. Peng, S. Lin and Z. Tang, *Angew. Chem., Int. Ed.*, 2019, **58**, 835–839.
81 Z. Wu, J. Liu, Y. Gao, H. Liu, T. Li, H. Zou, Z. Wang, K. Zhang, Y. Wang and H. Zhang, *J. Am. Chem. Soc.*, 2015, **137**, 12906–12913.
82 L. Ai, W. Jiang, Z. Liu, J. Liu, Y. Gao, H. Zou, Z. Wu, Z. Wang, Y. Liu and H. Zhang, *Nanoscale*, 2017, **9**, 12618–12627.
83 Z. Wang, Y. e. Shi, X. Yang, Y. Xiong, Y. Li, B. Chen, W. F. Lai and A. L. Rogach, *Adv. Funct. Mater.*, 2018, **28**, 1802848.
84 D. Li, G. Wang, L. Cheng, C. Wang and X. Mei, *ACS Omega*, 2018, **3**, 14755–14765.
85 D. Li, G. Wang, Y. Peng, Z. Chen, X. Gao, L. Cheng and X. Mei, *Nanoscale Adv.*, 2019, **1**, 1086–1095.
86 J. Li, J.-J. Zhu and K. Xu, *TrAC, Trends Anal. Chem.*, 2014, **58**, 90–98.
87 A. C. Bhowal, S. Pandit and S. Kundu, *J. Phys. D: Appl. Phys.*, 2019, **52**, 015302.
88 J. Bornacelli, C. Torres-Torres, H. Silva-Pereyra, G. Labrada-Delgado, A. Crespo-Sosa, J. Cheang-Wong and A. Oliver, *Sci. Rep.*, 2019, **9**, 5699.
89 G. S. Yuvasri, N. Goswami and J. Xie, *Principles and Applications of Aggregation-Induced Emission*, Springer, 2019, pp. 265–289.
90 G. Wang, T. Huang, R. W. Murray, L. Menard and R. G. Nuzzo, *J. Am. Chem. Soc.*, 2005, **127**, 812–813.
91 G. Wang, R. Guo, G. Kalyuzhny, J.-P. Choi and R. W. Murray, *J. Phys. Chem. B*, 2006, **110**, 20282–20289.
92 S. Maity, D. Bain and A. Patra, *J. Phys. Chem. C*, 2019, **123**, 2506–2515.
93 Y. Wang, Y.-e. Shi, T. Li, H. Wang, Y. Li, Y. Xiong, S. Peng and Z. Wang, *Nanoscale Adv.*, 2019, **1**, 834–839.
94 R. Jalili and A. Khataee, *Microchim. Acta*, 2019, **186**, 29.
95 Y. Guo, F. Cao, X. Lei, L. Mang, S. Cheng and J. Song, *Nanoscale*, 2016, **8**, 4852–4863.
96 W. Wei, Y. Lu, W. Chen and S. Chen, *J. Am. Chem. Soc.*, 2011, **133**, 2060–2063.
97 Z. Qing, X. He, D. He, K. Wang, F. Xu, T. Qing and X. Yang, *Angew. Chem., Int. Ed.*, 2013, **52**, 9719–9722.

98 C. Wang, L. Ling, Y. Yao and Q. Song, *Nano Res.*, 2015, **8**, 1975–1986.
99 A. W. Cook and T. W. Hayton, *Acc. Chem. Res.*, 2018, **51**, 2456–2464.
100 H.-H. Deng, K.-L. Li, Q.-Q. Zhuang, H.-P. Peng, Q.-Q. Zhuang, A.-L. Liu, X.-H. Xia and W. Chen, *Nanoscale*, 2018, **10**, 6467–6473.
101 Z. Wang, B. Chen, A. S. Susha, W. Wang, C. J. Reckmeier, R. Chen, H. Zhong and A. L. Rogach, *Adv. Sci.*, 2016, **3**, 1600182.
102 Z. Wu, H. Liu, T. Li, J. Liu, J. Yin, O. F. Mohammed, O. M. Bakr, Y. Liu, B. Yang and H. Zhang, *J. Am. Chem. Soc.*, 2017, **139**, 4318–4321.
103 K. D. M. Weerawardene, H. Häkkinen and C. M. Aikens, *Annu. Rev. Phys. Chem.*, 2018, **69**, 205–229.
104 Y. Du, H. Sheng, D. Astruc and M. Zhu, *Chem. Rev.*, 2019, DOI: 10.1021/acs.chemrev.8b00726.
105 Y. Huang, H. Feng, W. Liu, S. Zhang, C. Tang, J. Chen and Z. Qian, *J. Mater. Chem. B*, 2017, **5**, 5120–5127.
106 C. Wang, H. Cheng, Y. Huang, Z. Xu, H. Lin and C. Zhang, *Analyst*, 2015, **140**, 5634–5639.
107 N. K. Das, S. Ghosh, A. Priya, S. Datta and S. Mukherjee, *J. Phys. Chem. C*, 2015, **119**, 24657–24664.
108 H. Huang, H. Li, J.-J. Feng, H. Feng, A.-J. Wang and Z. Qian, *Sens. Actuators, B*, 2017, **241**, 292–297.
109 J. Liu, Q. M. Zhang, Y. Feng, Z. Zhou and K. Shih, *ChemPhysChem*, 2016, **17**, 225–231.
110 A. Baghdasaryan, R. Grillo, S. Roy Bhattacharya, M. Sharma, E. Reginato, H. Theraulaz, I. Dolamic, M. Dadras, S. Rudaz and E. Varesio, *ACS Appl. Nano Mater.*, 2018, **1**, 4258–4267.
111 B. Han, X. Hu, M. Yu, T. Peng, Y. Li and G. He, *RSC Adv.*, 2018, **8**, 22748–22754.
112 Y. Huang, W. Liu, H. Feng, Y. Ye, C. Tang, H. Ao, M. Zhao, G. Chen, J. Chen and Z. Qian, *Anal. Chem.*, 2016, **88**, 7429–7434.
113 H.-Y. Huang, K.-B. Cai, M. J. Talite, W.-C. Chou, P.-W. Chen and C.-T. Yuan, *Sci. Rep.*, 2019, **9**, 4053.
114 A. Ganguly, I. Chakraborty, T. Udayabhaskararao and T. Pradeep, *J. Nanopart. Res.*, 2013, **15**, 1522.
115 X. Liu, W. Ding, Y. Wu, C. Zeng, Z. Luo and H. Fu, *Nanoscale*, 2017, **9**, 3986–3994.
116 S. M. Lin, S. Geng, N. Li, N. B. Li and H. Q. Luo, *Talanta*, 2016, **151**, 106–113.
117 Y. Du, J. Fang, H. Wang and Y. Yang, *ACS Appl. Mater. Interfaces*, 2017, **9**, 11035–11044.
118 Y.-S. Borghei, M. Hosseini, M. Khoobi and M. R. Ganjali, *J. Fluoresc.*, 2017, **27**, 529–536.
119 Y. S. Borghei, M. Hosseini, M. Khoobi and M. R. Ganjali, *Luminescence*, 2017, **32**, 1045–1050.
120 N. Goswami, K. Zheng and J. Xie, *Nanoscale*, 2014, **6**, 13328–13347.
121 X. Su and J. Liu, *ACS Appl. Mater. Interfaces*, 2017, **9**, 3902–3910.
122 K. Khonkayan, S. Sansuk, S. Srijaranai, T. Tuntulani, C. Saiyasombat, W. Busayaporn and W. Ngeontae, *Microchim. Acta*, 2017, **184**, 2965–2974.
123 S. Sharma, K. K. Chakrahari, J.-Y. Saillard and C. Liu, *Acc. Chem. Res.*, 2018, **51**, 2475–2483.
124 M. Cui, G. Song, C. Wang and Q. Song, *Microchim. Acta*, 2015, **182**, 1371–1377.
125 T. Zhou, W. Xu, Q. Yao, T. Zhao and X. Chen, *Methods Appl. Fluoresc.*, 2015, **3**, 044002.
126 T. Zhou, Q. Yao, T. Zhao and X. Chen, *Talanta*, 2015, **141**, 80–85.
127 Y.-J. Lin, P.-C. Chen, Z. Yuan, J.-Y. Ma and H.-T. Chang, *Chem. Commun.*, 2015, **51**, 11983–11986.
128 S. Zhou, Y. Li, F. Wang and C. Wang, *RSC Adv.*, 2016, **6**, 38897–38905.
129 K. T. Prakash, N. Singh and V. Venkatesh, *Chem. Commun.*, 2019, **55**, 322–325.
130 J.-S. Shen, Y.-L. Chen, Q.-P. Wang, T. Yu, X.-Y. Huang, Y. Yang and H.-W. Zhang, *J. Mater. Chem. C*, 2013, **1**, 2092–2096.
131 X.-J. Zheng, R.-P. Liang, Z.-J. Li, L. Zhang and J.-D. Qiu, *Sens. Actuators, B*, 2016, **230**, 314–319.
132 A. Rotaru, S. Dutta, E. Jentzsch, K. Gothelf and A. Mokhir, *Angew. Chem., Int. Ed.*, 2010, **49**, 5665–5667.
133 B. Han, R. Xiang, X. Hou, M. Yu, T. Peng, Y. Li and G. He, *Anal. Methods*, 2017, **9**, 2590–2595.
134 F. Zhou, X. Cui, A. Shang, J. Lian, L. Yang, Y. Jin and B. Li, *Microchim. Acta*, 2017, **184**, 773–779.
135 Q. Song, Y. Shi, D. He, S. Xu and J. Ouyang, *Chem. – Eur. J.*, 2015, **21**, 2417–2422.
136 G. Liu, Y. Shao, J. Peng, W. Dai, L. Liu, S. Xu, F. Wu and X. Wu, *Nanotechnology*, 2013, **24**, 345502.
137 Y. Ling, N. Zhang, F. Qu, T. Wen, Z. F. Gao, N. B. Li and H. Q. Luo, *Spectrochim. Acta, Part A*, 2014, **118**, 315–320.
138 J. Feng, Y. Ju, J. Liu, H. Zhang and X. Chen, *Anal. Chim. Acta*, 2015, **854**, 153–160.
139 M. Zhao, L. Sun and R. M. Crooks, *J. Am. Chem. Soc.*, 1998, **120**, 4877–4878.
140 N. Vilar-Vidal, J. Rivas and M. A. Lopez-Quintela, *ACS Catal.*, 2012, **2**, 1693–1697.
141 L. Balogh and D. A. Tomalia, *J. Am. Chem. Soc.*, 1998, **120**, 7355–7356.
142 P. N. Floriano, C. O. Noble IV, J. M. Schoonmaker, E. D. Poliakoff and R. L. McCarley, *J. Am. Chem. Soc.*, 2001, **123**, 10545–10553.
143 R. Ghosh, U. Goswami, S. S. Ghosh, A. Paul and A. Chattopadhyay, *ACS Appl. Mater. Interfaces*, 2014, **7**, 209–222.
144 Z. Wang, A. S. Susha, B. Chen, C. Reckmeier, O. Tomanec, R. Zboril, H. Zhong and A. L. Rogach, *Nanoscale*, 2016, **8**, 7197–7202.
145 H. Zhang, X. Huang, L. Li, G. Zhang, I. Hussain, Z. Li and B. Tan, *Chem. Commun.*, 2012, **48**, 567–569.
146 Z. Yan, Q. Niu, M. Mou, Y. Wu, X. Liu and S. Liao, *J. Nanopart. Res.*, 2017, **19**, 235.
147 L. Xiaoqing, L. Ruiyi, L. Zaijun, S. Xiulan, W. Zhouping and L. Junkang, *New J. Chem.*, 2015, **39**, 5240–5248.
148 N. Goswami, A. Giri, M. Bootharaju, P. L. Xavier, T. Pradeep and S. K. Pal, *Anal. Chem.*, 2011, **83**, 9676–9680.

149 M. Chen, W. Li, H. Xiong, W. Wen, X. Zhang and S. Wang, *Microchim. Acta*, 2017, 1–8.
150 L. Zhao and Z. Ma, *Sens. Actuators, B*, 2017, **241**, 849–854.
151 H. Miao, D. Zhong, Z. Zhou and X. Yang, *Nanoscale*, 2015, **7**, 19066–19072.
152 R. Ghosh, A. K. Sahoo, S. S. Ghosh, A. Paul and A. Chattopadhyay, *ACS Appl. Mater. Interfaces*, 2014, **6**, 3822–3828.
153 L. Jin, Z. Zhang, A. Tang, C. Li and Y. Shen, *Biosens. Bioelectron.*, 2016, **79**, 108–113.
154 Y. Wang, Y. Cui, R. Liu, Y. Wei, X. Jiang, H. Zhu, L. Gao, Y. Zhao, Z. Chai and X. Gao, *Chem. Commun.*, 2013, **49**, 10724–10726.
155 W. Wang, F. Leng, L. Zhan, Y. Chang, X. X. Yang, J. Lan and C. Z. Huang, *Analyst*, 2014, **139**, 2990–2993.
156 Y. Ding, X. Li, C. Chen, J. Ling, W. Li, Y. Guo, J. Yan, L. Zha and J. Cai, *Sci. Rep.*, 2017, **7**, 9638.
157 Y. Qiao, T. Xu, Y. Zhang, C. Zhang, L. Shi, G. Zhang, S. Shuang and C. Dong, *Sens. Actuators, B*, 2015, **220**, 1064–1069.
158 X. Hu, X. Mao, X. Zhang and Y. Huang, *Sens. Actuators, B*, 2017, **247**, 312–318.
159 S. Biswas, J. T. Miller, Y. Li, K. Nandakumar and C. S. Kumar, *Small*, 2012, **8**, 688–698.
160 M. T. Reetz and W. Helbig, *J. Am. Chem. Soc.*, 1994, **116**, 7401–7402.
161 N. Vilar-Vidal, M. C. Blanco, M. A. López-Quintela, J. Rivas and C. Serra, *J. Phys. Chem. C*, 2010, **114**, 15924–15930.
162 S. Huseyinova, J. Blanco, F. l. G. Requejo, J. M. Ramallo-López, M. C. Blanco, D. Buceta and M. A. López-Quintela, *J. Phys. Chem. C*, 2016, **120**, 15902–15908.
163 N. Vilar-Vidal, J. R. Rey and M. A. López Quintela, *Small*, 2014, **10**, 3632–3636.
164 X. Jia, J. Li and E. Wang, *Small*, 2013, **9**, 3873–3879.
165 Z. Li, S. Guo and C. Lu, *Analyst*, 2015, **140**, 2719–2725.
166 X. Yuan, Z. Luo, Q. Zhang, X. Zhang, Y. Zheng, J. Y. Lee and J. Xie, *ACS Nano*, 2011, **5**, 8800–8808.
167 C. Vázquez-Vázquez, M. Bañobre-López, A. Mitra, M. A. López-Quintela and J. Rivas, *Langmuir*, 2009, **25**, 8208–8216.
168 R. K. Koninti, S. Satpathi and P. Hazra, *J. Phys. Chem. C*, 2018, **122**, 5742–5752.
169 H. Kawasaki, Y. Kosaka, Y. Myoujin, T. Narushima, T. Yonezawa and R. Arakawa, *Chem. Commun.*, 2011, **47**, 7740–7742.
170 C. Toh, X. Liu, P. Ho and J. Chen, *IEEE Trans. Magn.*, 2011, **47**, 4003–4006.
171 H. Haberland, M. Karrais, M. Mall and Y. Thurner, *J. Vac. Sci. Technol., A*, 1992, **10**, 3266–3271.
172 J. Chen, C. Tan, S. Chow, B. Liu and G. Chow, *J. Appl. Phys.*, 2005, **98**, 064306.
173 S. Pan, X. Zhang, W. Lu and S. F. Yu, *J. Mater. Chem. A*, 2018, **6**, 18687–18693.
174 M. Hyotanishi, Y. Isomura, H. Yamamoto, H. Kawasaki and Y. Obora, *Chem. Commun.*, 2011, **47**, 5750–5752.
175 X. Nie, H. Qian, Q. Ge, H. Xu and R. Jin, *ACS Nano*, 2012, **6**, 6014–6022.
176 S. Jalili, C. Mochani, M. Akhavan and J. Schofield, *Mol. Phys.*, 2012, **110**, 267–276.
177 M. Liu, X. Qiu, K. Hashimoto and M. Miyauchi, *J. Mater. Chem. A*, 2014, **2**, 13571–13579.
178 M. P. de Lara-Castells, A. W. Hauser, J. M. Ramallo-López, D. Buceta, L. J. Giovanetti, M. A. Lopez-Quintela and F. Requejo, *J. Mater. Chem. A*, 2019, **7**, 7489–7500.
179 B. Beguin, B. Denise and R. Sneeden, *J. Organomet. Chem.*, 1981, **208**, C18–C20.
180 Q. Tang, Y. Lee, D.-Y. Li, W. Choi, C. W. Liu, D. Lee and D.-e. Jiang, *J. Am. Chem. Soc.*, 2017, **139**, 9728–9736.
181 J. Fang, B. Zhang, Q. Yao, Y. Yang, J. Xie and N. Yan, *Coord. Chem. Rev.*, 2016, **322**, 1–29.
182 C. Sun, N. Mammen, S. Kaappa, P. Yuan, G. Deng, C. Zhao, J. Yan, S. Malola, K. Honkala and H. Häkkinen, *ACS Nano*, 2019, **13**, 5975–5986.
183 B. Zhang, A. Sels, G. Salassa, S. Pollitt, V. Truttmann, C. Rameshan, J. Llorca, W. Olszewski, G. Rupprechter and T. Bürgi, *ChemCatChem*, 2018, **10**, 5372–5376.
184 O. Lopez-Acevedo, K. A. Kacprzak, J. Akola and H. Häkkinen, *Nat. Chem.*, 2010, **2**, 329–334.
185 W. Chen and S. Chen, *Angew. Chem., Int. Ed.*, 2009, **48**, 4386–4389.
186 Y. Lu and W. Chen, *J. Power Sources*, 2012, **197**, 107–110.
187 Y. Lu, W. Wei and W. Chen, *Chin. Sci. Bull.*, 2012, **57**, 41–47.
188 W. Wei and W. Chen, *Int. J. Smart Nano Mater.*, 2013, **4**, 62–71.
189 Q.-Y. Zhang, Q.-F. Zhao, X.-M. Liang, X.-L. Wang, F.-X. Ma, B.-B. Suo, W.-L. Zou, H.-X. Han, Q. Song and Q. Wu, *Int. J. Hydrogen Energy*, 2018, **43**, 9935–9942.
190 M. Takahashi, H. Koizumi, W.-J. Chun, M. Kori, T. Imaoka and K. Yamamoto, *Sci. Adv.*, 2017, **3**, e1700101.
191 L. He, H. Liu, C.-X. Xiao and Y. Kou, *Green Chem.*, 2008, **10**, 619–622.
192 B. Sarkar, C. Pendem, L. N. Sivakumar Konathala, R. Tiwari, T. Sasaki and R. Bal, *Chem. Commun.*, 2014, **50**, 9707–9710.
193 A. A. Athawale and S. V. Bhagwat, *J. Appl. Polym. Sci.*, 2003, **89**, 2412–2417.
194 L. Hu, Y. Yuan, L. Zhang, J. Zhao, S. Majeed and G. Xu, *Anal. Chim. Acta*, 2013, **762**, 83–86.
195 D. Tang and J. Zhang, *RSC Adv.*, 2013, **3**, 15225–15236.
196 R. S. Dhayal, H. P. Chen, J. H. Liao, W. E. van Zyl and C. Liu, *ChemistrySelect*, 2018, **3**, 3603–3610.
197 S. S. Tafreshi, A. Roldan and N. H. de Leeuw, *J. Phys. Chem. C*, 2014, **118**, 26103–26114.
198 R. A. Hoyt, M. M. Montemore and E. Kaxiras, *J. Phys. Chem. Lett.*, 2018, **9**, 5339–5343.
199 V. V. Rostovtsev, L. G. Green, V. V. Fokin and K. B. Sharpless, *Angew. Chem.*, 2002, **114**, 2708–2711.
200 B.-H. Lee, C.-C. Wu, X. Fang, C. Liu and J.-L. Zhu, *Catal. Lett.*, 2013, **143**, 572–577.
201 Y. Zhong, Q. Wang, Y. He, Y. Ge and G. Song, *Sens. Actuators, B*, 2015, **209**, 147–153.
202 J. Liu, Z. Wu, Y. Tian, Y. Li, L. Ai, T. Li, H. Zou, Y. Liu, X. Zhang and H. Zhang, *ACS Appl. Mater. Interfaces*, 2017, **9**, 24899–24907.
203 G. Zhang, R. Wang, L. Shi, C. Zhang, Y. Zhang, Y. Zhou, C. Dong, G. Li and S. Shuang, *Sens. Actuators, B*, 2019, **279**, 361–368.

204 H. Cao, Z. Chen and Y. Huang, *Talanta*, 2015, **143**, 450–456.
205 L. Ruiyi, W. Huiying, Z. Xiaoyan, L. Xiaoqing, S. Xiulan and L. Zaijun, *New J. Chem.*, 2016, **40**, 732–739.
206 X. Hu, W. Wang and Y. Huang, *Talanta*, 2016, **154**, 409–415.
207 X. Yang, Y. Feng, S. Zhu, Y. Luo, Y. Zhuo and Y. Dou, *Anal. Chim. Acta*, 2014, **847**, 49–54.
208 D. Li, Z. Chen, Z. Wan, T. Yang, H. Wang and X. Mei, *RSC Adv.*, 2016, **6**, 34090–34095.
209 L. Lin, Y. Hu, L. Zhang, Y. Huang and S. Zhao, *Biosens. Bioelectron.*, 2017, **94**, 523–529.
210 S. M. Lin, S. Geng, N. Li, S. G. Liu, N. B. Li and H. Q. Luo, *Sens. Actuators, B*, 2017, **252**, 912–918.
211 H. Y. Zou, J. Lan and C. Z. Huang, *RSC Adv.*, 2015, **5**, 55832–55838.
212 N. K. Das, S. Ghosh, A. Priya, S. Datta and S. Mukherjee, *J. Phys. Chem. C*, 2015, **119**, 24657–24664.
213 Z. Shojaeifard, N. Heidari and B. Hemmateenejad, *Spectrochim. Acta, Part A*, 2019, **209**, 202–208.
214 J. Liu, B. Wang, M. Xu, L. Wang and Z. Zhou, *J. Lumin.*, 2017, **185**, 258–262.
215 D. Q. Feng, W. Zhu, G. Liu and W. Wang, *RSC Adv.*, 2016, **6**, 96729–96734.
216 L. Kong, X. Chu, W. Liu, Y. Yao, P. Zhu and X. Ling, *New J. Chem.*, 2016, **40**, 4744–4750.
217 Y. S. Lin, T. C. Chiu and C. C. Hu, *RSC Adv.*, 2019, **9**, 9228–9234.
218 Z.-C. Liu, J.-W. Qi, C. Hu, L. Zhang, W. Song, R.-P. Liang and J.-D. Qiu, *Anal. Chim. Acta*, 2015, **895**, 95–103.
219 D. Li, B. Li and S. I. Yang, *Anal. Methods*, 2015, **7**, 2278–2282.
220 Z. Shen, C. Zhang, X. Yu, J. Li, B. Liu and Z. Zhang, *Microchem. J.*, 2019, **145**, 517–522.
221 Y. Huang, W. Liu, H. Feng, Y. Ye, C. Tang, H. Ao, M. Zhao, G. Chen, J. Chen and Z. Qian, *Anal. Chem.*, 2016, **88**, 7429–7434.
222 P.-C. Chen, Y.-C. Li, J.-Y. Ma, J.-Y. Huang, C.-F. Chen and H.-T. Chang, *Sci. Rep.*, 2016, **6**, 24882.
223 J. Y. Ma, P. C. Chen and H. T. Chang, *Nanotechnology*, 2014, **25**, 195502.
224 U. Sivasankaran, J. Radecki, H. Radecka and K. Girish Kumar, *Luminescence*, 2019, **34**, 243–248.
225 Z. Wang, C. C. Zhang, J. Gao and Q. Wang, *J. Lumin.*, 2017, **190**, 115–122.
226 R. S. Aparna, J. S. Anjali Devi, P. Sachidanandan and S. George, *Sens. Actuators, B*, 2018, **254**, 811–819.
227 Z. Wang, R. Chen, Y. Xiong, K. Cepe, J. Schneider, R. Zboril, C. S. Lee and A. L. Rogach, *Part. Part. Syst. Charact.*, 2017, **34**, 1700029.
228 H. Li, J. Chang, T. Hou, L. Ge and F. Li, *Talanta*, 2016, **160**, 475–480.
229 H.-W. Zhu, W.-X. Dai, X.-D. Yu, J.-J. Xu and H.-Y. Chen, *Talanta*, 2015, **144**, 642–647.
230 Y. Nerthigan, A. K. Sharma, S. Pandey and H. F. Wu, *Microchim. Acta*, 2019, **186**(3), 130.
231 X. Zhang, Q. Liu, Y. Jin and B. Li, *ChemistrySelect*, 2019, **4**, 2398–2403.
232 R. Liu, L. Zuo, X. Huang, S. Liu, G. Yang, S. Li and C. Lv, *Microchim. Acta*, 2019, **186**, 250.
233 H. Jiang and X.-M. Wang, *Chin. J. Anal. Chem.*, 2017, **45**, 1776–1785.
234 Q. Song, Y. Shi, D. He, S. Xu and J. Ouyang, *Chem. – Eur. J.*, 2015, **21**, 2417–2422.
235 L. Zhao and Z. Ma, *Sens. Actuators, B*, 2017, **241**, 849–854.
236 C. Wang, S. Shu, Y. Yao and Q. Song, *RSC Adv.*, 2015, **5**, 101599–101606.
237 Y. Zhou, H. Wang, H. Zhang, Y. Chai and R. Yuan, *Anal. Chem.*, 2018, **90**, 3543–3549.
238 C. Muñoz-Bustos, A. Tirado-Guízar, F. Paraguay-Delgado and G. Pina-Luis, *Sens. Actuators, B*, 2017, **244**, 922–927.
239 Z. Gao, R. Su, W. Qi, L. Wang and Z. He, *Sens. Actuators, B*, 2014, **195**, 359–364.
240 N. Zhang, F. Qu, H. Q. Luo and N. B. Li, *Anal. Chim. Acta*, 2013, **791**, 46–50.
241 S. Xu, Y. Wang, D. Zhou, M. Kuang, D. Fang, W. Yang, S. Wei and L. Ma, *Sci. Rep.*, 2016, **6**, 39157.
242 W. Li, W. Li, Y. Hu, Y. Xia, Q. Shen, Z. Nie, Y. Huang and S. Yao, *Biosens. Bioelectron.*, 2013, **47**, 345–349.
243 Y. Hu, Q. Zhang, L. Xu, J. Wang, J. Rao, Z. Guo and S. Wang, *Anal. Bioanal. Chem.*, 2017, **409**, 6677–6688.
244 L. Wang, M. Wang, F. Shi, Z. Liu and X. Su, *Sens. Actuators, B*, 2017, **252**, 209–214.
245 H. Zhao, J. Dong, F. Zhou and B. Li, *Sens. Actuators, B*, 2017, **238**, 828–833.
246 Y. Zhang, Y. Li, C. Zhang, Q. Zhang, X. Huang, M. Yang, S. A. Shahzad, K. K.-W. Lo, C. Yu and S. Jiang, *Anal. Bioanal. Chem.*, 2017, **409**, 4771–4778.
247 Y. Hong, J. W. Y. Lam and B. Z. Tang, *Chem. Soc. Rev.*, 2011, **40**, 5361–5388.
248 T. Qing, C. Long, X. Wang, K. Zhang, P. Zhang and B. Feng, *Microchim. Acta*, 2019, **186**, 248.
249 M. Ye, Y. Yu, B. Lin, Y. Cai, Y. Cao, M. Guo and D. Zhu, *Sens. Actuators, B*, 2019, **284**, 36–44.
250 Q. Liu, Q. Lai, N. Li and X. Su, *Microchim. Acta*, 2018, **185**, 182.
251 Y. Huang, H. Feng, W. Liu, Y. Zhou, C. Tang, H. Ao, M. Zhao, G. Chen, J. Chen and Z. Qian, *Anal. Chem.*, 2016, **88**, 11575–11583.
252 X.-d. Wang, O. S. Wolfbeis and R. J. Meier, *Chem. Soc. Rev.*, 2013, **42**, 7834–7869.
253 X. Ma, Y. Wang, T. Zhao, Y. Li, L.-C. Su, Z. Wang, G. Huang, B. D. Sumer and J. Gao, *J. Am. Chem. Soc.*, 2014, **136**, 11085–11092.
254 L. Xiaoqing, L. Ruiyi, L. Xiaohuan and L. Zaijun, *RSC Adv.*, 2015, **5**, 48835–48841.
255 S. Uchiyama, Y. Matsumura, A. P. de Silva and K. Iwai, *Anal. Chem.*, 2003, **75**, 5926–5935.
256 F. H. C. Wong, D. S. Banks, A. Abu-Arish and C. Fradin, *J. Am. Chem. Soc.*, 2007, **129**, 10302–10303.
257 L. Wang, H. Miao, D. Zhong and X. Yang, *Anal. Methods*, 2016, **8**, 40–44.
258 T. Zhao, X.-W. He, W.-Y. Li and Y.-K. Zhang, *J. Mater. Chem. B*, 2015, **3**, 2388–2394.
259 M. Karimi, P. Sahandi Zangabad, A. Ghasemi, M. Amiri, M. Bahrami, H. Malekzad, H. Ghahramanzadeh Asl,

Z. Mahdieh, M. Bozorgomid and A. Ghasemi, *ACS Appl. Mater. Interfaces*, 2016, **8**, 21107–21133.
260 P. S. Zangabad, S. Mirkiani, S. Shahsavari, B. Masoudi, M. Masroor, H. Hamed, Z. Jafari, Y. D. Taghipour, H. Hashemi and M. Karimi, *Nanotechnol. Rev.*, 2018, **7**, 95–122.
261 Z. Liu, X. Jin, S. Zhang and Y. Tian, *Anal. Chem.*, 2019, **91**, 2488–2497.
262 S. Shahsavari, *J. Nanomed. Res.*, 2017, **5**, 000101.
263 R. Siegel, D. Naishadham and A. Jemal, *Ca-Cancer J. Clin.*, 2013, **63**, 11–30.
264 M. Shokeen and C. J. Anderson, *Acc. Chem. Res.*, 2009, **42**, 832–841.
265 H. Lyon, *Biotech. Histochem.*, 2002, **77**, 57–80.
266 X. Zhu, H. Shi, Y. Shen, B. Zhang, J. Zhao and G. Li, *Nano Res.*, 2015, **8**, 2714–2720.
267 K. Nakatani, *ChemBioChem*, 2004, **5**, 1623–1633.
268 X. Jia, J. Li, L. Han, J. Ren, X. Yang and E. Wang, *ACS Nano*, 2012, **6**, 3311–3317.
269 A. Abi and E. E. Ferapontova, *J. Am. Chem. Soc.*, 2012, **134**, 14499–14507.
270 X. Zhu, S. Liu, J. Cao, X. Mao and G. Li, *Sci. Rep.*, 2016, **6**, 19515.
271 K. Zheng, M. I. Setyawati, D. T. Leong and J. Xie, *ACS Nano*, 2017, **11**, 6904–6910.
272 S. Wang, Y. Wang, Y. Peng and X. Yang, *ACS Appl. Mater. Interfaces*, 2019, **11**, 8461–8469.
273 A. T. Simon, D. Dutta, A. Chattopadhyay and S. S. Ghosh, *ACS Omega*, 2019, **4**, 4697–4706.
274 S. Kundu and A. Patra, *Chem. Rev.*, 2016, **117**, 712–757.
275 H. Choi, Y.-S. Chen, K. G. Stamplecoskie and P. V. Kamat, *J. Phys. Chem. Lett.*, 2014, **6**, 217–223.
276 K. G. Stamplecoskie and P. V. Kamat, *J. Am. Chem. Soc.*, 2014, **136**, 11093–11099.
277 S. C. Erwin, L. Zu, M. I. Haftel, A. L. Efros, T. A. Kennedy and D. J. Norris, *Nature*, 2005, **436**, 91–94.
278 Z. Wang, B. Chen, M. Zhu, S. V. Kershaw, C. Zhi, H. Zhong and A. L. Rogach, *ACS Appl. Mater. Interfaces*, 2016, **8**, 33993–33998.
279 Y. Liu, D. Yao and H. Zhang, *ACS Appl. Mater. Interfaces*, 2017, **10**, 12071–12080.
280 H. Wang, Z. Wang, Y. Xiong, S. V. Kershaw, T. Li, Y. Wang, Y. Zhai and A. L. Rogach, *Angew. Chem., Int. Ed.*, 2019, **58**, 7040–7044.
281 Z. Wang, Y. Xiong, S. V. Kershaw, B. Chen, X. Yang, N. Goswami, W.-F. Lai, J. Xie and A. L. Rogach, *Chem. Mater.*, 2017, **29**, 10206–10211.
282 Y. e. Shi, X. Zhuang, L. Cao, S. Gou, Y. Xiong, W. F. Lai, Z. Wang and A. L. Rogach, *ChemNanoMat*, 2019, **5**, 110–115.

